

Review

# Emerging Energy Harvesting Technology for Electro/Photo-Catalytic Water Splitting Application

Jianfei Tang <sup>1</sup>, Tianle Liu <sup>2</sup>, Sijia Miao <sup>3</sup>  and Yuljae Cho <sup>2,\*</sup>

<sup>1</sup> Department of Materials Science and Engineering, University of Michigan, Ann Arbor, MI 48109, USA; jianfei@umich.edu

<sup>2</sup> University of Michigan-Shanghai Jiao Tong University Joint Institute, Shanghai Jiao Tong University, 800 Dong Chuan Road, Minghang District, Shanghai 200240, China; tyrion\_l2017@sjtu.edu.cn

<sup>3</sup> School of Optical and Electronic Information, Huazhong University of Science and Technology, Wuhan 430074, China; u201714349@hust.edu.cn

\* Correspondence: yuljae.cho@sjtu.edu.cn; Tel.: +86-21-34206765 (ext. 5441)

**Abstract:** In recent years, we have experienced extreme climate changes due to the global warming, continuously impacting and changing our daily lives. To build a sustainable environment and society, various energy technologies have been developed and introduced. Among them, energy harvesting, converting ambient environmental energy into electrical energy, has emerged as one of the promising technologies for a variety of energy applications. In particular, a photo (electro) catalytic water splitting system, coupled with emerging energy harvesting technology, has demonstrated high device performance, demonstrating its great social impact for the development of the new water splitting system. In this review article, we introduce and discuss in detail the emerging energy-harvesting technology for photo (electro) catalytic water splitting applications. The article includes fundamentals of photocatalytic and electrocatalytic water splitting and water splitting applications coupled with the emerging energy-harvesting technologies using piezoelectric, piezophototronic, pyroelectric, triboelectric, and photovoltaic effects. We comprehensively deal with different mechanisms in water splitting processes with respect to the energy harvesting processes and their effect on the water splitting systems. Lastly, new opportunities in energy harvesting-assisted water splitting are introduced together with future research directions that need to be investigated for further development of new types of water splitting systems.

**Keywords:** energy harvesting; piezoelectricity; pyroelectricity; triboelectricity; photovoltaics; electrocatalysis; photocatalysis; water splitting



**Citation:** Tang, J.; Liu, T.; Miao, S.; Cho, Y. Emerging Energy Harvesting Technology for Electro/Photo-Catalytic Water Splitting Application. *Catalysts* **2021**, *11*, 142. <https://doi.org/10.3390/catal11010142>

Received: 29 December 2020

Accepted: 16 January 2021

Published: 19 January 2021

**Publisher's Note:** MDPI stays neutral with regard to jurisdictional claims in published maps and institutional affiliations.



**Copyright:** © 2021 by the authors. Licensee MDPI, Basel, Switzerland. This article is an open access article distributed under the terms and conditions of the Creative Commons Attribution (CC BY) license (<https://creativecommons.org/licenses/by/4.0/>).

## 1. Introduction

Energy and environment issues are the two critical challenges that we human beings are currently confronting [1]. The fast depletion of fossil fuels and growing population have brought up more concerns about energy crisis, and meanwhile increasing emissions of greenhouse gases have resulted in accelerated global warming and climate changes over the world [2,3]. At present, developing sustainable energy resources has emerged as the main topic of interest around the world [1,4,5].

Hydrogen, as a clean, renewable, and high energy density fuel, is considered as an ideal alternative to fossil fuels. Its easy storage and applications in fuel cells and combustion engines have demonstrated the great potential of hydrogen as a promising energy carrier [6,7]. Today, 95% of hydrogen is generated from fossil fuel-based products, with 4% from electricity and 1% from biomass [8]. In the pursuit of a clean and carbon-free energy resource, water splitting from renewable energy resources for hydrogen evolution has gained increasing research attention over the years [1,8–11]. However, the practical performance of industrial-scale hydrogen generation through two primary approaches of water splitting, electrolysis, and photolysis, is less than satisfactory. Electrolysis consumes

a tremendous amount of electricity, primarily generated from fossil fuels; photolysis is severely restricted in efficiency by the rapid recombination of charge carriers within photocatalysts [12,13]. Hence, developing highly efficient renewable energy systems is crucial for sustainable hydrogen production.

Energy harvesting technology, which aims to supply power, primarily electricity, with sustainable energy, can provide the ideal energy resources for hydrogen generation through water splitting [14,15]. To date, energy harvesting of heat, solar power, and mechanical energy has been intensively studied [9,16–19]. On the basis of piezoelectric, pyroelectric, triboelectric, or photovoltaic effects, ambient energy present in the environment is collected and converted into electrical energy through the energy harvester. For piezoelectric and pyroelectric effects, electrical charges are generated from charge separation and polarization of the material induced by external vibration or heat, triboelectric charges are induced on material surface through surface friction, and photovoltaic electricity originates from the separation of light-induced excitons. The generated electrical energy is either directly coupled in the water splitting process or is transmitted from the energy harvesting device to a photo (electro) catalytic water splitting system, i.e., electrolyzer, to produce hydrogen. Compared to conventional electrocatalytic or photocatalytic approaches, water splitting coupled with energy harvesting technology exhibits the following advantages: (i) utilization of ambient environmental energy demonstrating a sustainable and carbon-free system, (ii) synergy effects between conventional photolysis or electrolysis process and energy harvesting approaches such as piezoelectric effects leading to improved hydrogen generation, and (iii) diversity and versatility of energy harvesting technology enabling effective water splitting application under different conditions.

In this review, we summarize recent progress in energy harvesting technology coupled with water splitting applications. To provide general ideas on energy harvesting technology-assisted water splitting, we comprehensively discuss mechanical, thermal, and photon energy harvesting in five different sub-chapters. First, fundamentals and mechanism of photocatalytic and electrocatalytic water splitting are explained. Second, recent trends in energy harvesting technologies, including piezoelectric, piezo-phototronic, pyroelectric, triboelectric, and photovoltaic effects, are introduced. Water splitting systems coupled with emerging energy harvesting technology are reviewed with particular emphasis. Finally, we discuss new opportunities involving new materials regarding interaction for energy harvesting with the water splitting process, as well as the outlook of potential research directions of energy harvesting materials and devices for water splitting applications.

## 2. Fundamentals of Water Splitting

Photocatalysis and electrocatalysis are the two most frequently used means to achieve renewable energy-driven water splitting. In this section, the fundamentals of photocatalytic and electrocatalytic water splitting are introduced.

### 2.1. Photocatalytic Water Splitting

Photocatalytic water splitting utilizes solar energy from sun radiation and achieves hydrogen production from water, during which solar energy is converted to chemical energy. Currently, hydrogen production by a photocatalytic system can be achieved through two primary approaches. In one approach, water is split into  $H_2$  and  $O_2$  on a single light-responsive photocatalyst under the excitation of incident light [20]. The other approach is to set up a two-step excitation process using two different photocatalysts, where  $H_2$  and  $O_2$  are formed separately through the two processes. In this approach, a pair of redox mediators, composed of an electron donor and an electron acceptor, are applied to connect two photocatalytic processes together and transfer the electrons [21]. Through both approaches, water goes through redox reaction, leading to the formation of  $H_2$  and  $O_2$ .

As we can expect from the reaction scheme shown in Figure 1a, the electronic structure of the semiconductor photocatalyst plays a key role in photocatalysis. Typically, the semiconductor photocatalyst has a conduction band (CB), a valence band (VB), and a

bandgap energy  $E_g$ —the energy difference between the CB and VB. Without excitation, both the electrons and holes are in valence band. Photocatalytic water splitting originates with an electron excitation process within such an electronic structure. When the semiconductor photocatalyst is exposed to light with energy equal to or higher than its bandgap energy  $E_g$ , the electrons in the VB are stimulated to the CB, leaving holes in the VB. This process is regarded as the electron-hole generation and separation. The photo-induced electrons and holes are relatively free to move within the semiconductor. Then, if the electrons and holes could migrate to the surface of the photocatalyst, they would respectively oxidize or reduce the reactants absorbed on the semiconductor,  $H_2O$  and  $H^+$ , respectively, in water splitting. This process is denoted as the electron-hole transportation and surface catalytic reactions. The following equations illustrates the general mechanism of photocatalytic water splitting.

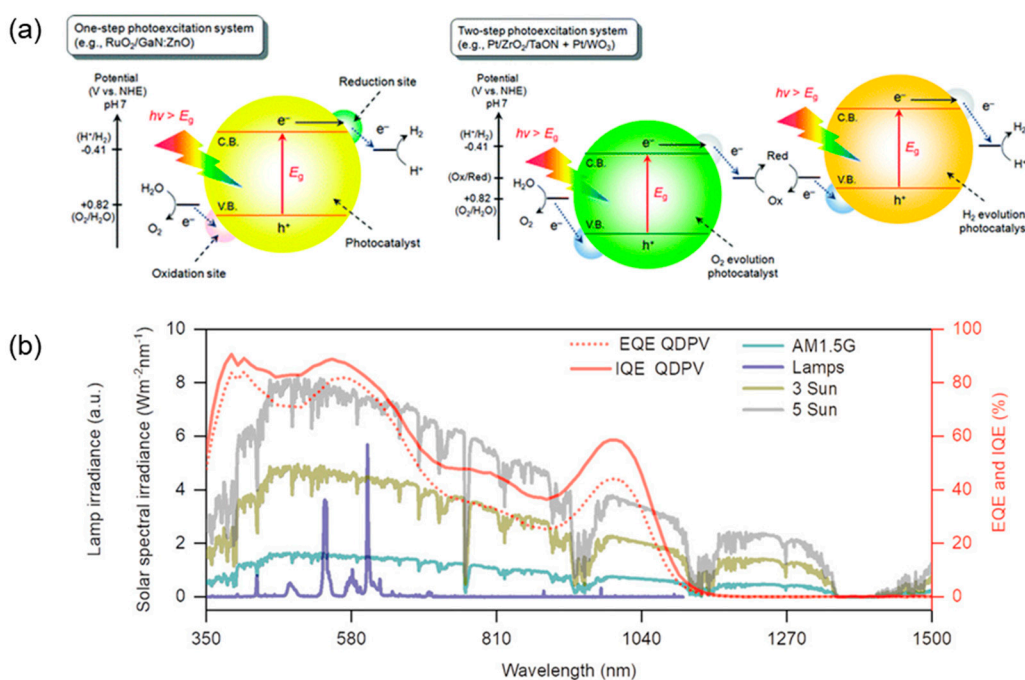
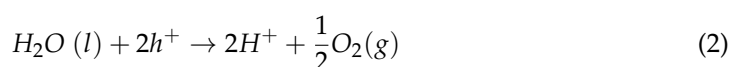
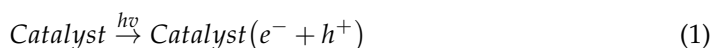


**Figure 1.** (a) Reaction scheme of one-step and two-step excitation process of photocatalytic water splitting. (b) The spectra of solar irradiance, a fluorescent lamp (1000 lux), and examples of the external and internal quantum efficiency spectra (1.24 eV lead sulphide quantum dots). Reproduced from [21], Copyright 2010, American Chemical Society. Reproduced from [22], Copyright 2020, Wiley-VCH Verlag GmbH & Co. KGaA, Weinheim.

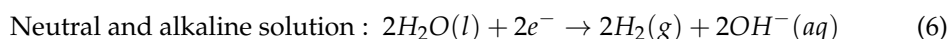
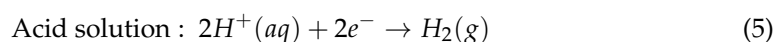
Equation (1) describes the process of electron-hole generation and separation. Equations (2) and (3) correspond to the oxidation and reduction surface catalytic reaction, respectively. However, the generated electrons and holes would not always migrate to the surface of the photocatalyst and react ideally. The photo-generated electrons and holes can also recombine in bulk or on the surface of the semiconductor within a very short time, releasing energy in the form of heat or photons. Such process is electron-hole recombination, as is illustrated in Equation (4). This process can lead to large amount of energy loss, resulting in low photocatalytic efficiency [23]. The fast recombination problem of electron-hole pair is a hot spot that attracts great

research interest, and continuous efforts have been made to restrain the recombination of charge carriers in photocatalysts and promote photocatalytic activity. On another hand, efficiency of photocatalysts under sun light irradiation is largely affected by the band gap and light wavelength. Figure 1b shows the spectra of solar irradiance. Visible light and infrared radiation represent the majority solar radiation energy. Effective photocatalysts generally have a band gap larger than 2 eV, which corresponds to light wavelength of 620 nm; moreover, to utilize more energy from the solar radiation, the band gap of photocatalyst should be lower than 3.1 eV to harvest visible light. At present, many photocatalysts, such as TiO<sub>2</sub>, have a wide bandgap, which leads to low light adsorption, with band gap narrowing through modifying the photocatalyst having become as a topic of interest. Application of two-step excitation process as illustrated above, addition of sacrificial reagent and electrolytes for improved electron transfer, metal loading and doping for tuning electronic structure, emerging of hybrid energy harvesting materials and devices, etc., have been widely investigated.

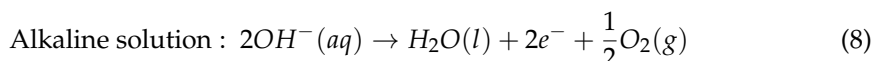
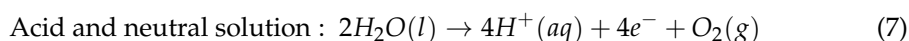
## 2.2. Electrocatalytic Water Splitting

Electrocatalytic water splitting ( $H_2O(l) \rightarrow H_2(g) + \frac{1}{2}O_2(g)$ ) typically consists of two half-reactions, the hydrogen evolution reaction (HER) which occurs on the cathode and oxygen evolution reaction (OER) on the anode, as Equations (5)–(8) describe. Depending on the pH, the two electrode reactions can have different expressions:

- Cathode reaction (HER):



- Anode reaction (OER):



In terms of electrocatalytic reaction mechanism, HER and OER can have different reaction routes, yet share a similar underlying mechanism. In HER, the reaction starts from electrochemical adsorption of H atoms, often called Volmer reaction, where proton sources react with electrons on the catalyst surface (denoted as M) to generate adsorbed protons  $H^*$  in a  $M - H^*$  form. Then, hydrogen gas may be formed via electrochemical desorption (Heyrovsky reaction), where  $M - H^*$  react with another proton diffused to the catalyst surface, or chemical desorption (Tafel reaction), where two adjacent  $H^*$  combine together on the surface to generate H<sub>2</sub>, or both. In OER, the mechanism is not fully understood, yet common points among the proposed mechanisms are present. Similar to HER, during OER, the catalyst surface (M) adsorbs  $OH^-$  or desorbs protons to form the reaction intermediates in forms of  $M - OH$ ,  $M - O$ , and  $M - OOH$  sequentially, leading to the final formation of O<sub>2</sub> (g). Through another proposed route, O<sub>2</sub> (g) can also be produced via the direct combination of two MO intermediates [24,25].

According to the mechanisms discussed above, for both HER and OER, the rate of absorption and desorption of the catalyst surface plays a key role in determining the overall reaction rate. This behavior is illustrated in the Sabatier principle, stating that the optimal catalytic activity of electrocatalysis is achieved on a catalyst surface with an intermediate bonding energy (or free adsorption energy) for the  $M - X$  reaction agents. To be specific, if the interaction between catalysts and reaction intermediates is too strong, the products cannot desorb fast and hence block the reaction by occupying active sites, and if it is too weak, few reactive agents adsorb on the catalysts, slowing down the reaction [25]. This can also be seen in a  $\log j_0$  vs.  $\Delta G_{H^*}$  volcano plot, where  $j_0$  is exchange current density and

$\Delta G_{H^*}$  is the Gibbs free adsorption energy (Figure 2). An ideal catalyst should have  $\Delta G$  equal or close to zero.

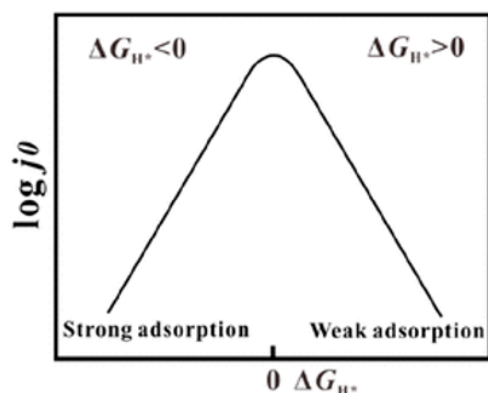


**Figure 2.** Relationship of  $\log j_0$  vs.  $\Delta G_{H^*}$  for adsorbed protons  $H^*$ . Reproduced from [26], Copyright 2019, American Chemical Society.

Thermodynamic and kinetics view can reveal more about the electrocatalytic reaction and its rate. The overall water splitting  $H_2O(l) \rightarrow H_2(g) + \frac{1}{2}O_2(g)$  has a positive  $\Delta G^0 = 237.13 \text{ kJ} \cdot \text{mol}^{-1}$  and  $\Delta E^0 = 1.23 \text{ V}$ . Under standard conditions, thermodynamic potential of 1.23 V is required to achieve electrocatalytic water splitting. However, the sluggish kinetics of HER and OER require additional over potential  $\eta$  to achieve specific current density. The over potential  $\eta$  is defined as the difference between the applied potential and the equilibrium potential, as Equation (9) shows below:

$$\eta = E - E_{eq} \quad (9)$$

Equilibrium potential  $E_{eq}$  refers to the potential at which forward reaction and backward reaction of the water splitting reaction are in an equilibrium state. Over potential  $\eta$  reflects the energy required to overcome the kinetic energy barrier. As described in Equation (10), the current density increases exponentially as over potential increases, where  $b$  is the Tafel slope.

$$\eta = b \log(j/j_0) \quad (10)$$

The Tafel slope describes relationships between current density and over potential, which is related with charge transfer between reactants and the catalyst. In HER, at 25 °C,  $b = 29, 39, 116 \text{ mV decade}^{-1}$  if the rate determining step is Tafel, Heyrovsky, and Volmer reaction, respectively [26]. Apart from over potential, ohmic potential drop in external circuits should also be considered in practical application.

### 3. Emerging Energy Harvesting Technology for Water Splitting

#### 3.1. Piezoelectric Energy Harvesting-Assisted Water Splitting

Utilization of a piezoelectric effect for catalytic applications has attracted tremendous attention since its breakthrough in the 1970s [27]. An induced electric field due to the dipole polarization tuned the catalytic rate by effectively modulating barrier height at a semiconductor interface and enhanced charge carrier separation, which resulted in improved catalytic performance [28,29]. In addition, spatial separation of charge carriers led to oxidation and reduction reactions preferred at different sites with respect to the direction of dipole polarization [30]. This phenomenon was demonstrated by density functional theory (DFT) simulations that the dipole polarization field is able to mediate the adsorption and desorption of reactants and products on the surface of piezoelectric catalysts, which suggests that it is possible to overcome fundamental limitations of catalysis, which was theoretically estimated by the Sabatier principle [31]. Recently, the piezoelectric energy harvesting coupled with electrochemical processes has demonstrated the modulation of

charge-carrier conduction at the heterojunction between the piezoelectric material and a chemical solution [32–35]. Piezoelectric energy harvesting introduced a new strategy to enable and improve photo(electro)catalytic water splitting by harnessing mechanical energy using various dimensional nanomaterials, such as zinc oxide (ZnO) and barium titanium oxide (BaTiO<sub>3</sub>) one-dimensional (1D) nanomaterials, and molybdenum disulfide (MoS<sub>2</sub>) two-dimensional (2D) nanomaterials. The basic mechanism of the piezoelectric energy harvesting-driven water splitting is that the physical deformation induced by the mechanical energy induces an electric field due to the polarized electric dipoles. Driven by the induced electric potential, free electrons and holes or photo-generated charges are separated and transferred to the opposite directions, prior to recombination. As a result, more electrons and holes can be collected at the surface of catalysts for the redox reaction. To induce a piezoelectric polarization or potential, mechanical strain needs to be applied to the piezoelectric materials. Among various approaches to induce the piezoelectric potential, one of the most practical ways is using ultrasound irradiation because mechanical vibrations are the most available mechanical energy around us in our daily lives [28,36–41].

In 2010, Hong et al. demonstrated enhanced HER and OER using piezoelectric ZnO microfibers and BaTiO<sub>3</sub> micro-dendrites by harvesting ultrasonic vibrations [33]. Figure 3a shows underlying mechanisms for the piezoelectric energy harvesting-assisted water splitting. Upon the application of ultrasonic vibrations, strain is induced to ZnO microfibers and BaTiO<sub>3</sub> micro-dendrites, and therefore a piezoelectric potential is generated. Reduction and oxidation reaction occur by this strain-induced electric potential over the standard redox potential of water (1.23 eV). The piezoelectric potential-induced charges are transferred to species, for example, water molecules adsorbed on the surface of the piezoelectric material, and thus hydrogen and oxygen gases are generated. However, residual charges or potential lower than the standard redox potential of water (1.23 eV) do not contribute to the generation of hydrogen and oxygen from water. Figure 3b–d illustrates hydrogen and oxygen production with and without the application of ultrasonic vibrations. When ultrasonic vibration was applied (0–40 min), rapid hydrogen and oxygen production were obtained at an initial rate of  $3.4 \times 10^{-3} \times 10^{-6}$  (ppm) per second and  $1.7 \times 10^{-3} \times 10^{-6}$  (ppm) per second, respectively. Similar to ZnO microfibers, H<sub>2</sub> evolution of approximately  $1.25 \times 10^{-2} \times 10^{-6}$  (ppm) per second in the first vibration event (0–50 min) was observed using BaTiO<sub>3</sub> micro-dendrites in pure water. This result demonstrates that the electrocatalysts, i.e., ZnO and BaTiO<sub>3</sub>, participated in the direct water splitting reaction by providing electrons and holes induced by the piezoelectric potential.

In the following work, Starr et al. employed piezoelectric Pb(Mg<sub>1/3</sub>Nb<sub>2/3</sub>)O<sub>3</sub>-32PbTiO<sub>3</sub> (PMN-PT) film for the water splitting application [34]. First, the author provided a theoretical analysis that the induced piezo-potential through the material deformation creates favorable electronic energy band alignments for promoting red-ox reactions of the water. As shown in Figure 3e, when the potential of the cathode is higher than that of the proton-reduction potential, electrons are transferred to protons and generate H<sub>2</sub> gases. Similarly, O<sub>2</sub> gases are generated at the anode by receiving electrons transferred when the energy levels of the anode are deep enough due to the induced piezoelectric potential. These reactions will cease eventually when the piezoelectricity-induced surface charges are depleted and thus electron energy levels are below the redox reaction potentials. In addition to H<sub>2</sub> generation measurement with respect to the time, in this work, the author further demonstrated H<sub>2</sub> production as a function of the piezoelectric potential. As the induced piezoelectric potential increased, the rate of H<sub>2</sub> production also increased, which further demonstrated the role of the piezoelectric potential in redox reaction for water splitting, as shown in Figure 3f.

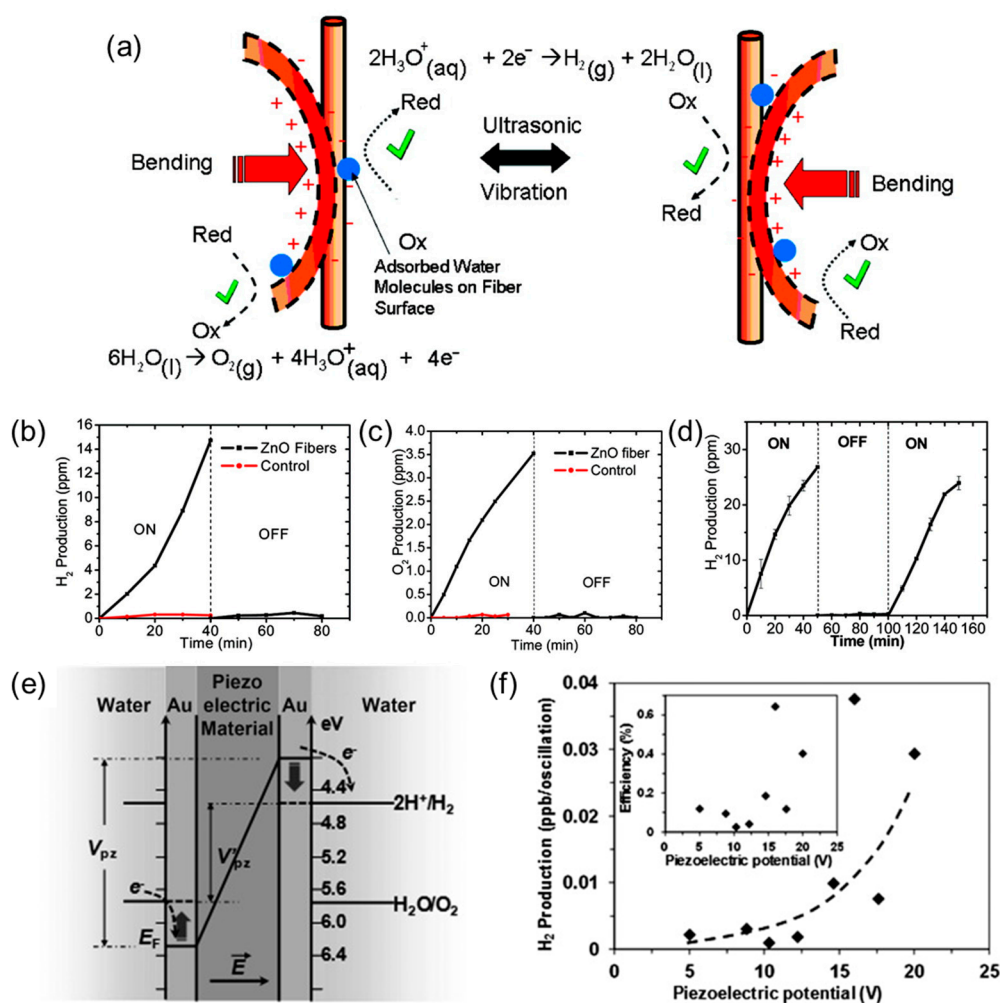


**Figure 3.** (a) Illustration of  $H_2$  and  $O_2$  generation mechanisms assisted by the piezoelectric energy harvesting. Evolution of (b)  $H_2$  and (c)  $O_2$  as a function of time using the piezoelectric ZnO nanowires. (d)  $H_2$  evolution performance of as-synthesized  $BaTiO_3$  dendrite. (e) Schematics of piezoelectric potential drive water splitting mechanism. (f)  $H_2$  production rate as a function of piezoelectric potential where the inset shows the corresponding catalytic efficiency. (a–d) Reproduced from [33], Copyright 2010, American Chemical Society. (e,f) Reproduced from [34], Copyright 2012, Wiley-VCH Verlag GmbH & Co. KGaA, Weinheim.

Other fascinating materials for piezoelectric energy harvesting-assisted water splitting are a group of two-dimensional (2D) materials, in particular, layered transition metal dichalcogenides (TMDs), for example, molybdenum disulfide ( $MoS_2$ ), tungsten disulfide ( $WS_2$ ), and tungsten diselenide ( $WSe_2$ ) [42–46]. The group of 2D TMDs nanomaterials possess superior piezoelectricity with high flexibility due to the nature of the materials, which provides an ability to withstand enormous strain/stress applied. Ever since the first demonstration of piezoelectricity in  $MoS_2$  experimentally, there have been significant research on the piezoelectric effects of 2D TMD nanomaterials [47–52]. Among them, in particular, TMDs have attracted tremendous attentions for photocatalysts and electrocatalysts, attributed to rich edge active sites for hydrogen evolution reaction (HER) [42–44,53].

In 2019, Li et al. reported water splitting devices using various types of few-layer TMDs, i.e.,  $MoS_2$ ,  $WS_2$ , and  $WSe_2$  [54]. Periodic mechanical strain is applied to the materials by using ultrasonic vibration, which causes deformation of the materials. Consequently, the mechanical deformation leads to the generation of piezoelectric field that enhances catalytic water splitting processes. As shown in Figure 4a, hydrogen was not produced without a catalyst, whereas all of the TMDs nanomaterials produced  $H_2$  from water under ultrasonic vibration. The amount of  $H_2$  evolution showed the order of  $MoS_2 > WS_2 > WSe_2$  with

the  $H_2$  evolution rate of approximately 29, 15, and 11  $\mu\text{mol}\cdot\text{g}^{-1}\cdot\text{h}^{-1}$  for  $\text{MoS}_2$ ,  $\text{WS}_2$ , and  $\text{WSe}_2$ , respectively (Figure 4a,b). Interestingly, the catalytic performances of TMDs were in good agreement with the intensity of the piezoresponse of each TMD materials, which exhibited 4.04, 3.25, and 1.51 p.m.  $\text{V}^{-1}$  for  $\text{MoS}_2$ ,  $\text{WS}_2$ , and  $\text{WSe}_2$ , respectively. In addition, negligible  $H_2$  evolution was observed when a bulk  $\text{MoS}_2$  sheet was employed for the catalytic water splitting (Figure 4c). These combined results—piezoresponse of TMDs and negligible  $H_2$  evolution from bulk  $\text{MoS}_2$ —highlight that the piezoelectric potential in TMDs materials indeed plays a crucial role in catalytic reactions. Furthermore, the author claimed that the piezocatalytic performance of the TMD samples were significantly improved by employing noble nanoparticles, for example, Pt and Au, demonstrating  $H_2$  production rate of 82.4 and 53.8  $\mu\text{mol}\cdot\text{g}^{-1}\cdot\text{h}^{-1}$  for Pt- $\text{MoS}_2$  and Au- $\text{MoS}_2$ , respectively. Finally, the author proposed the underlying mechanism of enhanced catalytic water splitting performance assisted by the piezoelectric effect. Figure 4d illustrates dipole polarization in the piezoelectric 2D TMD materials under the external stress. Similar to the piezoelectric-assisted water splitting mechanism in 1D nanostructures, the piezoelectric field generated by the dipole polarization in 2D materials system facilitates transport of free electrons and holes towards catalytic reaction sites where hydrogen and oxygen are produced by reduction and oxidation processes.

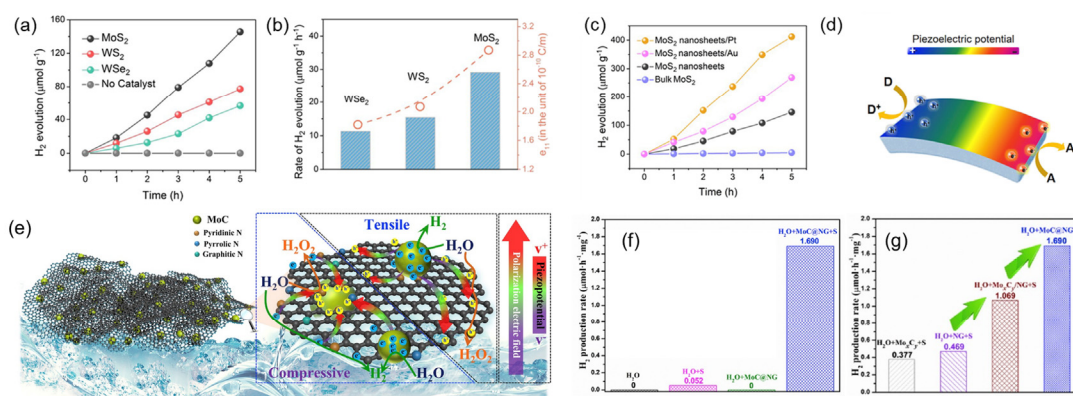


**Figure 4.** (a) Amounts of  $H_2$  production with respect to the different transition metal dichalcogenide (TMD) nanosheets. (b) The corresponding  $H_2$  production rate and the  $e_{11}$  values calculated. (c) Amounts of  $H_2$  production with different materials, namely, bulk  $\text{MoS}_2$ ,  $\text{MoS}_2$  nanosheets,  $\text{MoS}_2$  nanosheets/Pt, and  $\text{MoS}_2$  nanosheets/Au. (d) Schematics of the piezoelectric potential induced catalytic reactions in 2D TMD nanomaterials under mechanical force. (e) Schematics of piezoelectric effect driven  $H_2$  mechanism. Comparison of  $H_2$  production (f) with the bare N-doped graphene (NG) layer and (g) with the  $\text{MoC@NG}$ . (a–d) Reproduced from [54], Copyright 2019, Elsevier. (e–g) Reproduced from [55], Copyright 2020, Elsevier.

Following this work, other interesting works using the strategy of employing nanoparticles to enhance catalytic water splitting performances together with piezoelectric 2D TMD materials have been introduced. For example, in 2020, Feng et al. demonstrated  $H_2$  production from pure water by employing a piezoelectric N-doped graphene (NG) with molybdenum carbide (MoC) quantum dots [55]. Figure 4e illustrates a possible mechanism of piezoelectric energy harvesting-driven  $H_2$  production from pure water by using  $\text{MoC@NG}$  composite. When mechanical vibrations are triggered by ultrasonic irradiation, a dipole polarization electric field is induced due to the mechanical deformation, which results in the application of tensile and compressive strain to the  $\text{MoC@NG}$  composite. Under the strained conditions, the  $\text{MoC@NG}$  composite exhibits  $H_2$  evolution by reducing  $H_2O$  at pyridinic and pyrrolic N–Mo–C sites and graphitic N–Mo–C sites in tensile and compressive regions, respectively, whereas the oxidation of  $H_2O$  was observed at graphitic N sites and pyridinic and pyrrolic N sites on the graphene domain in tensile and compressive regions, respectively, producing  $H_2O_2$ . Figure 4f shows experimental results of  $H_2$  evolution with different material combinations and conditions. In the ab-

sence of ultrasonic irradiation, no detectable level of H<sub>2</sub> was produced by water itself or MoC@NG composite (black and green bar, respectively). A small amount of H<sub>2</sub>, the production rate of  $\approx 0.052 \mu\text{mol}\cdot\text{h}^{-1}\cdot\text{mg}^{-1}$ , was detected in pure water under ultrasonic irradiation. This is because pure water was cleaved to produce H and OH, and they were dimerized to form H<sub>2</sub> and H<sub>2</sub>O<sub>2</sub>, respectively, under ultrasonic vibrations [56,57]. As expected, MoC@NG generated the highest production rate of H<sub>2</sub> up to  $1.690 \mu\text{mol}\cdot\text{h}^{-1}\cdot\text{mg}^{-1}$ , which is attributed to the piezoelectric field generated by the ultrasonic vibrations. In the article, the author performed counter experiments to prove enhanced H<sub>2</sub> evolution rate assisted by the piezoelectric effect by harvesting mechanical energy. Notably, employment of piezoelectric NG as an electrocatalyst exhibited higher H<sub>2</sub> production rate compared to the one without piezoelectric NG (black bar vs. purple, red, and blue bars), as shown in Figure 4g. In particular, the piezoelectric effect with MoC exhibited superior water splitting performance, which demonstrates the obvious synergistic effect of the piezoelectric field and electrocatalytic behaviors.

In spite of its promising future, the development stage of piezoelectric effect on catalytic water splitting is still premature. Furthermore, the piezoelectric potential generated by the mechanical energy is relatively weak, which limits the potential water splitting application comparing to the electrocatalytic or photocatalytic water splitting processes. For piezoelectric energy harvesting-assisted water splitting alone, a balance between piezoelectric properties and conductivity needs to be addressed to further enhance H<sub>2</sub> evolution rate.

### 3.2. Piezo-Phototronic Energy Harvesting-Assisted Water Splitting

The further advanced concept of water splitting applications has been introduced by utilizing piezo-phototronic effect. Piezo-phototronic effect is used to tune charge transport mechanisms through a coupling of semiconducting, photoexciting, and piezoelectric properties simultaneously [58–62]. In this sub-chapter, we will introduce the concept of piezo-phototronic effect to enhance the production of H<sub>2</sub> and O<sub>2</sub> in water splitting applications. An employment of single-component narrow-bandgap photocatalysts offers more benefits compared to the hybrid photocatalysts, which are a combination of a narrow bandgap material with noble metals if photo-generated charges can be separated and transferred prior to recombination. Therefore, the underlying motivation of using piezo-phototronic effect in the water splitting application is to overcome inefficient charge transfer caused by rapid recombination of photo-excited electron–hole pairs in a narrow-bandgap photocatalysts by utilizing a piezo-phototronic effect [36,56,63,64].

Recently, Zhao et al. reported cadmium sulfide (CdS) nanorod (NR)-based piezo-phototronic water splitting devices for H<sub>2</sub> generation from pure water [56]. In spite of disadvantages of charge transport with the narrow bandgap material, the author employed CdS nanorods to harvest visible light ranging from 400 to 700 nm. In this work, the synergistic effects of photocatalytic and piezoelectric properties of CdS nanorod demonstrated significant enhancement in H<sub>2</sub> evolution rates, as shown in Figure 5a where L and S stand for the application of visible light source and ultrasonic vibration, respectively. Under only visible light irradiation, there was no observable amount of generated H<sub>2</sub> gases, regardless of the existence of CdS nanorods, indicating that photo-generated excitons were mostly recombined. In contrast, when both light and sound were applied to the water splitting system, CdS nanorods generated increased amount of H<sub>2</sub> generation with the aid of the piezo-photoelectric effect to efficiently separate and transport photo-generated charge carriers. However, the author could not observe a difference in H<sub>2</sub> generation in both systems without and with CdS nanorods under only ultrasonic, suggesting that CdS nanorods are not a sonocatalyst. These processes are illustrated in Figure 5b, showing the mechanism of piezo-phototronic effect—with the existence of both visible light irradiation and ultrasonic vibration, CdS nanorods produce increased amount of H<sub>2</sub> without any sacrificial agent compared to H<sub>2</sub> generated by only light irradiation or ultrasonic vibration. This is attributed to the separation of photo-excited electron and hole pairs, by the piezoelectric field, which otherwise would be recombine prior to their dissociation. However, Cd used

in this work is toxic and harmful to humans and nature, and it is desirable to substitute harmful substances with environmentally friendly ones.

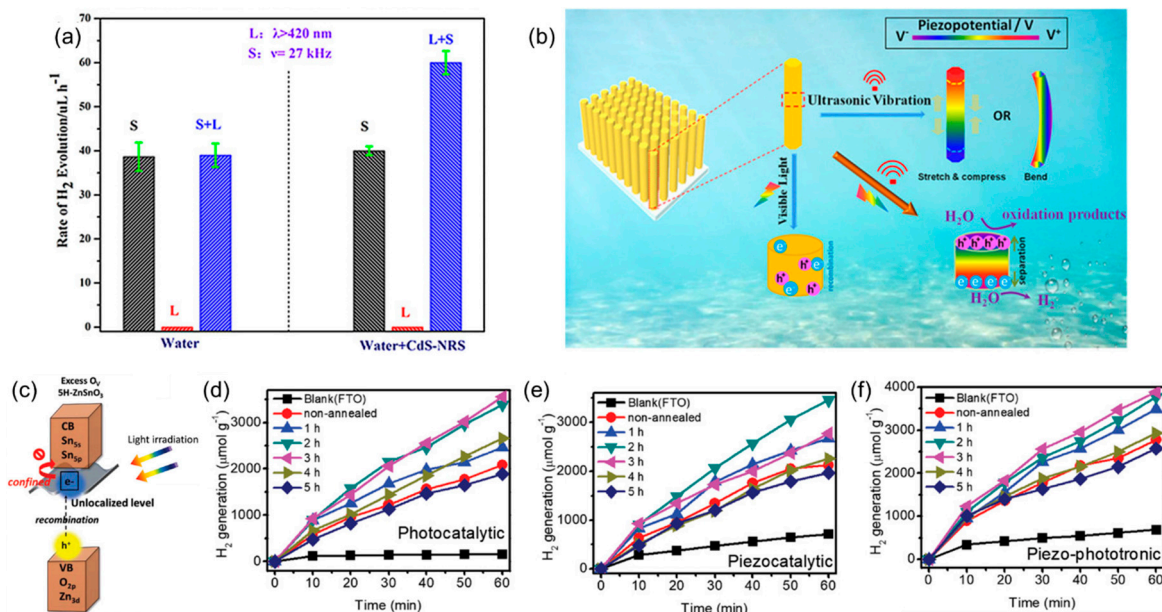
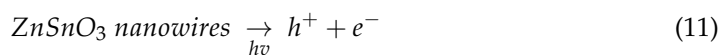


**Figure 5.** (a) H<sub>2</sub> production rate at different conditions. (b) Mechanism of CdS-NRs piezo-phototronic effect in H<sub>2</sub> generation under visible light and ultrasonic excitation. (c) Schematics of ZnSnO<sub>3</sub> water splitting system with the piezo-phototronic effect. The amount of H<sub>2</sub> production of ZnSnO<sub>3</sub> NWs as a function of time under (d) only light irradiation, (e) only ultrasonic vibration, and (f) both light and ultrasonic vibration simultaneously. (a,b) Reproduced from [56], Copyright 2018, Wiley-VCH Verlag GmbH & Co. KGaA, Weinheim. (c–f) Reproduced from [63], Copyright 2019, Wiley-VCH Verlag GmbH & Co. KGaA, Weinheim.

Similarly, Wang et al. reported the piezoelectric-assisted photocatalytic effect in ZnSnO<sub>3</sub> nanowires (NW), as shown in Figure 5c [63]. In this article, nanowires composed of environmentally friendly materials, such as zinc (Zn) and tin (Sn), were synthesized using a hydrothermal method. The synthesized environmentally friendly ZnSnO<sub>3</sub> nanowires exhibited piezo-photoelectric effects that can utilize both mechanical vibrations and light to produce higher volume of H<sub>2</sub>. The author systematically compared three possible catalytic activities in ZnSnO<sub>3</sub> nanowires with thermal annealing time ranging from 1 to 5 h. Figure 5d–f illustrates the generated H<sub>2</sub> production rate by (i) photocatalytic (Figure 5d), (ii) piezocatalytic (Figure 5e), and (iii) piezo-photocatalytic behavior (Figure 5f). Through either photocatalytic or piezocatalytic activity, a maximum amount of 3562.2 and 3453.1 μmol·g<sup>-1</sup> of H<sub>2</sub> was generated, respectively. The synergistic effect on generating H<sub>2</sub> 3882.5 μmol·g<sup>-1</sup> was observed when both light irradiation and mechanical vibrations were present. This is attributed to the separation of electron–hole pairs by the piezoelectric effect prior to their recombination, demonstrating the synergistic piezo-phototronic effect. Equations (11)–(14) illustrate the piezophotocatalytic processes. First, light-induced excitons are separated by interband and intraband transitions, i.e., from the valence band to the conduction band (Equation (11)). The separated electrons and holes are transferred to opposite directions due to the piezoelectric field induced by the mechanical stress. Consequently, methanol or water molecule receives a hole and generated a proton (H<sup>+</sup>), as Equations (12) and (13) describe. Finally, the proton reacts with the electron, and through this, H<sub>2</sub> gas is produced (Equation (14)).





In addition to ZnSnO<sub>3</sub> nanowires, other nanomaterials without heavy metals have demonstrated the piezo-phototronic effect for the water splitting applications, such as a typical ferroelectric nanocrystal zinc oxide (ZnO) and metal niobate (e.g., KNbO<sub>3</sub>, NaNbO<sub>3</sub>, and AgNbO<sub>3</sub>). Piezoelectric ZnO nanowires are one of the materials that have attained tremendous attention [37,65–67]. Chen et al. reported a direct Z-scheme water splitting strategy using the piezo-phototronic effect in ZnO-WO<sub>3-x</sub> nanoarrays, as shown in Figure 6a [65]. The piezoelectric effect significantly improved transport of photogenerated charges between ZnO and WO<sub>3-x</sub>. Figure 6b illustrates the principal mechanism of the piezo-phototronic effect in ZnO nanostructures, which modulate photo/electrocatalytic water splitting performance. By the piezoelectric field, the junction barrier height is changed, leading to efficient photo-generated charge transport to the electrodes [66]. Together with ZnO nanorods/wires, KNbO<sub>3</sub> and NaNbO<sub>3</sub> are promising candidates for the piezo-phototronic effect-assisted water splitting applications. In 2013, Singh and Khare employed synthesized NaNbO<sub>3</sub> to enhance the efficiency of photoelectrochemical water splitting through the piezo-phototronic effect, as shown in Figure 6c [68]. Under mechanical strain, NaNbO<sub>3</sub> generated the built-in piezoelectric potential, which facilitated dissociation of photo-generated charges. This led to enhanced photocurrent density from 0.78 to 1.02 mA·cm<sup>-2</sup> compared to the NaNbO<sub>3</sub> without mechanical strain. Recently, KNbO<sub>3</sub> was employed for the piezo-phototronic water splitting application by Yu et al., as shown in Figure 6d. At the optimal poling configuration, the author demonstrated a significantly enhanced device performance, attributed to the piezo-phototronic effect [69].

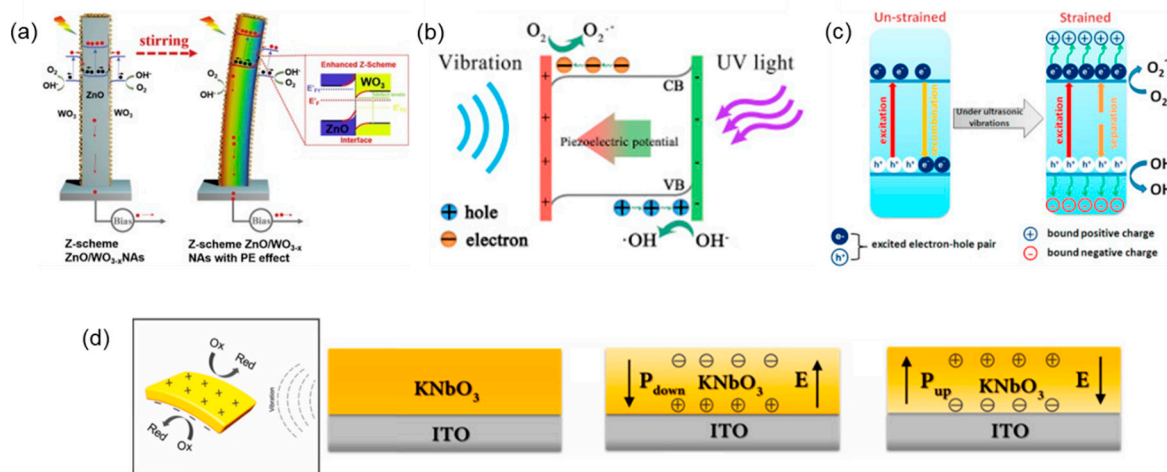


**Figure 6.** (a) Schematic illustration of piezo-phototronic effect in ZnO for water splitting. (b) The mechanism diagram of harvesting both photon and vibration energy, i.e., piezo-phototronic effect. (c) Schematics of the exciton separation mechanism in the un-strained and strained NaNbO<sub>3</sub>. (d) Schematic illustration of the piezo-catalytic reaction mechanism for the KNbO<sub>3</sub> (without poling, with negative poling and with positive poling conditions). (a) Reproduced from [65], Copyright 2019, Elsevier. (b) Reproduced from [66], Copyright 2019, Elsevier. (c) Reproduced from [68], Copyright 2017, Elsevier (d) Reproduced from [69], Copyright 2019, Elsevier.

### 3.3. Pyroelectric Energy Harvesting-Assisted Water Splitting

Heat is one of the attractive energy sources due to its omnipresence in the surrounding environment and the fact that it results from a variety of industrial applications [9]. Pyroelectric materials can generate usable electric charges with a high energy conversion efficiency under repeated heating and cooling. In theory, pyroelectric materials could deliver a higher energy conversion efficiency than photocatalytic materials do on the basis

of the photovoltaic effect. A mechanism of pyroelectricity is that a change in temperature induces the polarization of the material and consequently voltage is generated across the crystal [70,71]. The intensity of dipole polarization decreases when the temperature of the material is elevated. Consequently, electric charges are released on the surface of the materials [72]. On the other hand, when temperature decreases, the intensity of dipole polarization is increased, which results in reversed current flow as electric charges are attracted to the surface with higher polarization. When it comes to a water splitting application of the pyroelectric effect, the amount of charges ( $Q$ ) generated by a temperature change ( $\Delta T$ ) in a pyroelectric material can be described by Equation (15), where  $p$  is the pyroelectric coefficient ( $\text{Cm}^{-2}\cdot\text{K}^{-1}$ ) and  $A$  is the surface area ( $\text{m}^2$ ) of the material. In addition, the potential ( $V$ ) induced by the pyroelectric effect depends on thickness ( $h$ ) of the material used, as shown in Equation (16), where  $\epsilon_{33}$  is the relative permittivity of the material and  $\epsilon_0$  is the permittivity of free space.

$$Q = p \cdot A \cdot \Delta T \quad (15)$$

$$V = \frac{p \cdot h \cdot \Delta T}{\epsilon_0 \epsilon_{33}} \quad (16)$$

As shown in Equations (15) and (16), the amount of charges is proportional to the surface area, and generated potential is proportional to thickness, suggesting that a judicious design of a device structure and pyroelectric elements are needed to optimize electrolysis using the pyroelectric effect. For example, a sufficient potential to initiate a water splitting process can be induced by adjusting the thickness of the material while maximizing the surface charges through the surface area modifications. A theoretical work on pyroelectric water splitting was performed by Fang et al. in 2010 using numerical simulations on a  $0.9\text{PbMg}_{1/3}\text{Nb}_{2/3}-0.1\text{PbTiO}_3$  thin film pyroelectric converter that harvests nanoscale thermal radiation [73]. The simulations showed that an efficiency of 1.35% and an electrical power output of  $6.5 \text{ mW}\cdot\text{cm}^{-2}$  were achieved for cold and hot sources at 283 and 383 K, respectively. Following this work, in 2012, Huang et al. reported an energy density of  $128 \text{ mJ}\cdot\text{cm}^{-3}$  harvested in pyroelectric  $\text{Ba}_{1-x}\text{Sr}_x\text{TiO}_3$  ( $x = 0.35$ ) film under thermal cycling between 2 and 77 °C [74]. Recently, Xie et al. reported pyro-driven control of an electrochemical process and its application to water-splitting by using an external pyroelectrically-induced charge source with lead zirconate titanate (PZT) and polyvinylidene fluoride (PVDF) thin films [9]. To date, two types of pyroelectric energy harvesting system have been employed for water splitting applications: (i) internally positioned pyroelectric (IPP) approach, and (ii) externally positioned pyro-electrolysis (EPP). In this sub-section, we review the two types of water splitting systems on the basis of various nanomaterial dimensions [31,75–78].

- Internally positioned pyroelectric (IPP) approach.

First of all, the IPP approach provides several benefits as follows: (i) using finely dispersed pyroelectric particulates suspended in the electrolyte, it is possible to enable the area of the pyroelectric to be increased, and therefore, (ii) more available charges for hydrogen production. In simulation works on a pyroelectric induced water splitting process, Kakekhani et al. developed a DFT model of a ferroelectric lead titanate ( $\text{PbTiO}_3$ ) material and examined the impact of thermal cycling of the ferroelectric as it is heated above and cooled below Curie temperature ( $T_C$ ) in the presence of water molecules [31]. The work showed that cycling between the low temperature ferroelectric state and high temperature paraelectric state provides scope to harvest thermal fluctuations and produces hydrogen. Theoretical studies have shown that it is possible to switch the ferroelectric into paraelectric phase (and vice versa) of  $\text{PbZr}_x\text{Ti}_{1-x}\text{O}_3$  (PZT) and  $\text{BaTiO}_3$  (BTO) by modulating the temperature near the ferroelectric  $T_C$  by using the pyroelectric effect [31]. Through the periodic temperature changes,  $\text{H}_2\text{O}$  molecules are dissociated to produce bound atomic hydrogen on the negatively charged surface, and hydrogen atoms form  $\text{H}_2$  at low and high temperature. In addition to the theoretical and simulation works,

there have been experimental demonstration on water splitting applications assisted by the pyroelectric energy harvesting [76,77,79,80]. In particular, Xu et al. recently presented experimental data of  $\text{Ba}_{0.7}\text{Sr}_{0.3}\text{TiO}_3$  (BST) powders suspended in an electrolyte, achieving a hydrogen production of  $46.89 \mu\text{mol}$  per gram of the powder after 36 thermal cycles above and below its  $T_C$  [75]. Pyroelectric two-dimensional black phosphorene has also been reported as a charge source under thermal cycling for both hydrogen generation and dye decomposition [81]. We discuss more details on these two examples in the following sections.

First, Xu et al. demonstrated the pyroelectric effect-assisted  $\text{H}_2$  generation using BST nanoparticles. The temperature variations ( $\Delta T$ ) in the pyroelectric BST generate electrons and holes on each surface of the material. The pyroelectric-induced positive charges oxidize  $\text{H}_2\text{O}$  molecules adsorbed on the surface of BST nanoparticles, which subsequently produces the hydrogen ion ( $\text{H}^+$ ) and oxygen  $\text{O}_2$ . Then, the  $\text{H}^+$  ion reacts with the pyroelectric-induced negative charge to form hydrogen ( $\text{H}_2$ ), as shown in the Equations (17) and (18).



As shown in Figure 7a–c, the author demonstrated the pyroelectric assisted catalytic water splitting performance of BST under two conditions: with and without the addition of sacrificial methanol. The yield of pyroelectric-assisted hydrogen generation was a negligibly small value of  $0.75 \mu\text{mol}\cdot\text{g}^{-1}$  after 36 thermal cycles without the addition of methanol, whereas the rate of hydrogen evolution for BST with the addition of sacrificial methanol is around  $1.3 \mu\text{mol}\cdot\text{g}^{-1}$  per thermal cycle (298–323 K, 10 min). In addition, Figure 7c shows the yield of  $\text{H}_2$  increased up to  $46.89 \mu\text{mol}\cdot\text{g}^{-1}$  as the number of thermal cycles increased, suggesting the promising future of the pyroelectric assisted water splitting applications. The mechanism of the IPP type of the pyroelectric assisted water splitting involves two steps: (i) charge carriers are generated by the pyroelectric effect due to temperature changes/fluctuation, and then (ii) the generated charge carriers participate in redox reactions, resulting in generation of  $\text{H}_2$  gases. By harvesting thermal energy, in the form of temperature fluctuation, through the pyroelectric effect, water splitting application has been demonstrated, suggesting a significant impact to the field of renewable energy and sustainable society.

Because ferroelectric materials are both piezoelectric and pyroelectric, 2D structured ferroelectric materials can also be used for pyroelectric energy harvesting-assisted water splitting applications [81,82]. Recently, You et al. employed a 2D few-layer black phosphorene (2D-BP) to harness temperature variation for water splitting applications where the author adopted the IPP method [81]. As shown in Figure 7d, few-layer 2D-BP possesses a suitable electronic band structure for pyroelectricity-assisted electrocatalytic hydrogen generation. The conduction band minimum is higher, i.e., more negative, than the  $\text{H}^+/\text{H}_2$  reduction potential, which is favorable for  $\text{H}_2$  generation from water [83,84]. Similar to BST nanoparticles, the few-layer 2D-BP induces negative and positive charges at each side of the material upon the cold–hot alternation excitation. These charges will be transferred to the reactant molecules and induce the redox reaction. This process further demonstrates that the pyroelectric assisted electrocatalytic water splitting is a viable method to harness wasted heat energy to produce useful hydrogen gases regardless of material dimensions. In the set of following experiments, the author demonstrated the rate of  $\text{H}_2$  production,  $22.5 \mu\text{mol}\cdot\text{g}^{-1}$  per thermal cycle, and  $0.54 \text{ mmol}$  of the total  $\text{H}_2$  production per gram in 24 h with the temperature variation between 15 and  $65^\circ\text{C}$ , as shown in Figure 7e.

- Externally positioned pyro-electrolysis (EPP):

Another approach to utilize pyroelectricity is through externally positioned pyro-electrolysis (EPP). Different from the IPP method, which inevitably involves pH changes and has low efficiency at the current stage [81,82], the EPP provides several advantages: (i) The generation of  $\text{H}_2$  and  $\text{O}_2$  occurs at each electrode, which is spatially separated, and

therefore there is no need for gas separation. (ii) The charges provided by the external pyroelectric device can be readily collected compared to the IPP one, i.e., higher efficiency. The first experimental demonstration of external water electrolysis using pyroelectricity was carried out using thin layers of PZT, demonstrating its potential for H<sub>2</sub> generation. Figure 8a illustrates the experiment settings that the author used for the EPP approach and Figure 8b demonstrates the generation of H<sub>2</sub> gas in the EPP water splitting system [9]. In the following work, Zhang et al. demonstrated the EPP method to generate H<sub>2</sub> gas using a PZT sheet, which directly provided charges for pyroelectric water splitting as shown in Figure 8c [78]. The basic mechanism of the EPP involves three main steps: (i) by the pyroelectric effect, positive and negative charges are generated at opposite side of surfaces (bottom image of Figure 8c); (ii) the alternative current (AC) signal is changed to the direct current (DC) signal using a rectifier; (iii) the charges provided by the pyroelectric device then transferred to the cathode and anode to generate H<sub>2</sub> and O<sub>2</sub> gas, respectively. In the experiment, the author used a 0.5 M of KOH to demonstrate the generation of hydrogen and oxygen by the pyroelectric effect. Figure 8d shows the generated H<sub>2</sub> as a function of time (1–6 h), exhibiting an H<sub>2</sub> evolution increase from 0.38 μmol to 3.93 μmol. The total amount of H<sub>2</sub> and O<sub>2</sub> gas production after 6 h is shown in Figure 8e. The ratio of H<sub>2</sub> and O<sub>2</sub> is approximately 2:1, which is reasonably predictable from the reaction  $2\text{H}_2\text{O} \rightarrow 2\text{H}_2 + \text{O}_2$ . In this work, both H<sub>2</sub> and O<sub>2</sub> gases were simultaneously generated by utilizing charges induced by the externally connected pyroelectric energy harvesting device. Despite a nature of the bulk material employed in the work, i.e., much smaller surface area than that of the nanomaterials, pyroelectric induced water splitting using the EPP method, overall demonstrated promising results for future water splitting applications.

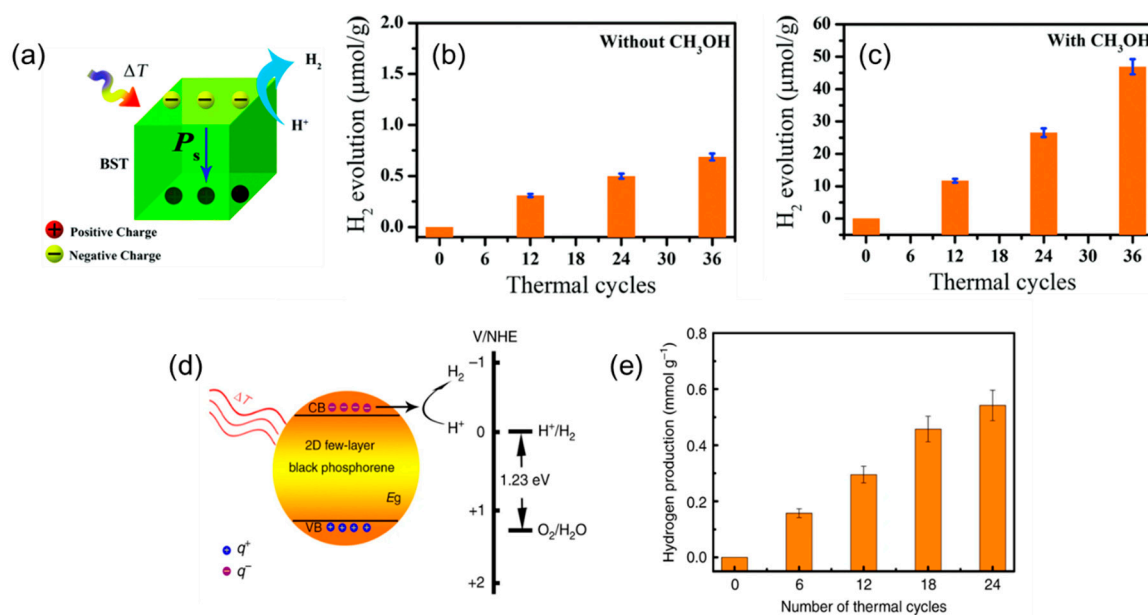


**Figure 7.** (a) The working mechanism of the pyroelectric effect on hydrogen evolution. The pyroelectric energy harvesting-assisted H<sub>2</sub> evolution under temperature fluctuations (b) without and (c) with methanol. (d) Schematics of H<sub>2</sub> generation by the pyroelectric effect. (e) Pyroelectric effect assisted electrocatalytic H<sub>2</sub> production. (a–c) Reproduced from [75], Copyright 2018, Royal Society of Chemistry. (d,e) Reproduced from [81], Copyright 2018, Springer Nature.

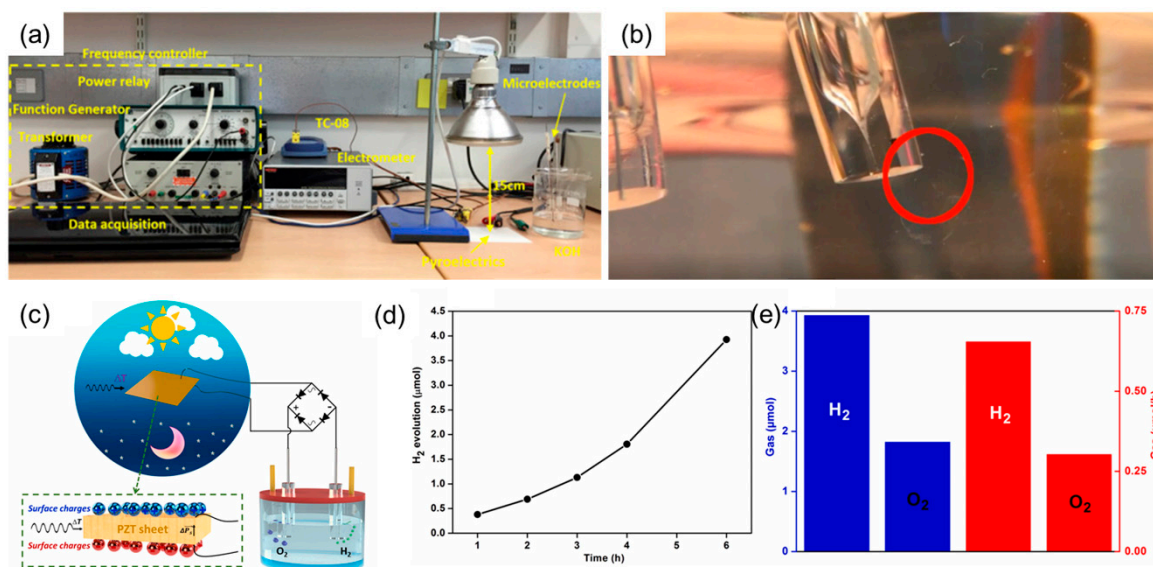


**Figure 8.** (a) Experimental setup for splitting of water using pyroelectrics. (b) Continuous hydrogen bubble production during thermal cycling. (c) Schematic of externally positioned pyro-electrolysis (EPP) pyroelectric energy harvesting for water splitting. (d) H<sub>2</sub> evolution from the EPP pyroelectric water splitting. (e) The amount and evolution rate of H<sub>2</sub> and O<sub>2</sub> gases attained for 6 h. (a,b) Reproduced from [9], Copyright 2017, Elsevier. (c–e) Reproduced from [78], Copyright 2017, Elsevier.

### 3.4. Triboelectric Energy Harvesting-Assisted Water Splitting

The last type of the mechanical energy harvesting in water splitting applications to introduce is a triboelectric energy harvester (often called triboelectric nanogenerator (TENG)), which was invented by Wang et al. [85]. Similar to the piezoelectric energy harvesting, the generator utilizes mechanical energy to induce charges on the surface of the materials through the triboelectric effect. The biggest merits of the TENG are that (i) it can generate high voltage, (ii) there are wider choices of materials as most of polymer materials show triboelectricity, (iii) the device structure is simple, and (iv) it is easy and cost-effective to fabricate. Therefore, TENGs have attracted significant research interest ever since its invention [86–89].

The integration of triboelectric energy generator into the photoelectrochemical water splitting system has been actively researched [90–94]. In this configuration, the energy generator provides a necessary bias to activate the electrolysis process. For example, Wei et al. demonstrated TENG-driven photoelectrochemical water splitting [90]. Figure 9a,b shows the water splitting system with the TENG under light illumination, which followed and promoted the previous work performed by Li et al. in Figure 9e,f. By harnessing external mechanical energy, the TENG provided high enough potential and current to anode and cathode, and therefore a photoelectrochemical cell generated H<sub>2</sub> gas, as shown in Figure 9c. In particular, when the plentiful of mechanical energy was provided to the TENG, i.e., high rotation speed (over 120 rpm), the water splitting system exhibited the direct electrolysis of water. The peak rate of H<sub>2</sub> evolution was approximately 6.67 μL·min<sup>-1</sup> with the aid of the TENG, demonstrating the triboelectric energy harvesting as the potential medium to facilitate water splitting processes. The TiO<sub>2</sub> anode was decorated by Au nanoparticles, which localized the optical energy by the surface plasmonic resonance effect. By coupling with the TENG, the hot electrons injection from Au to TiO<sub>2</sub> conduction band was enhanced, which resulted in improved water splitting performance. Lastly, TENG-driven water splitting was applied to a drug delivery system, which was demonstrated by Song et al. The generated H<sub>2</sub> and O<sub>2</sub> through the water splitting process enable delivery of a drug solution to the target, as shown in Figure 9g [94].

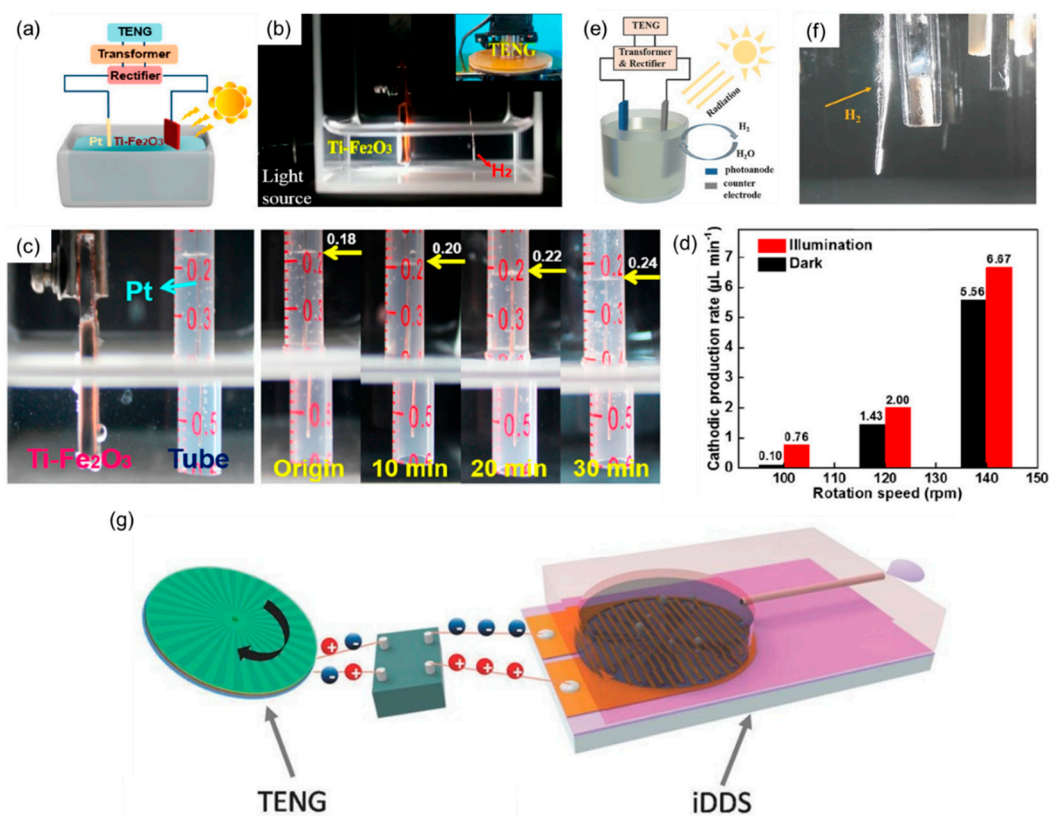


**Figure 9.** (a) Schematics of the triboelectric nanogenerator (TENG)-driven water splitting system and (b) digital image. (c) Digital images of the gas collection tube at different time. (d) Cathodic production rate as a function of rotation speeds to generate currents and potentials from the TENG. (e) Schematics of the TENG-driven photoelectrochemical (PEC) hybrid cell. (f) Photograph of water splitting process. (g) Schematic illustration of the TENG-driven water splitting for the drug delivery system. (a–d) Reproduced from [90], Copyright 2018, American Chemical Society. (e,f) Reproduced from [92], Copyright 2017, Wiley-VCH Verlag GmbH & Co. KGaA, Weinheim. (g) Reproduced from [94], Copyright 2017, Wiley-VCH Verlag GmbH & Co. KGaA, Weinheim.

### 3.5. Photovoltaic Energy Harvesting-Assisted Water Splitting

Solar energy, as the most abundant renewable source of energy, can also be harvested for hydrogen production as well [95]. The photovoltaic device harvests solar power and converts it to electrical energy, which is then transported to an electrolyzer to generate hydrogen through water splitting. Such a photovoltaic (PV)–electrolysis system typically contains two separate components, the light absorption PV component and the water splitting electrolysis component wired to the PV component [96]. The efficiency of PV component and the coupling effects between the two components are the keys in determining the solar-to-hydrogen (STH) efficiency of the PV–electrolysis system [97]. Developments in highly efficient solar cells have provided massive improvements in STH efficiencies. Luo et al. combined state-of-the-art perovskite tandem solar cell with NiFe-layered double hydroxide electrodes to form a PV–electrolysis system with a 12.3% STH efficiency [98]. Bonke et al. reported a 22% solar to hydrogen energy conversion efficiency using concentrator photovoltaic modules with commercially available InGaP/GaAs/Ge three-junction cells, which has a quoted 37% solar to electrical power conversion efficiency (PCE) [99]. In theory, the solar-to-hydrogen efficiency of PV–electrolysis system can reach up to 90–95% of the solar cell power conversion efficiency, demonstrating significant improvement possibilities [100–102].

The efficiency loss between solar cell PV efficiency and the actual solar-to-hydrogen efficiency is mainly attributed to the mismatch between electrolysis voltage and that of PV cells [97,99]. The thermodynamics of water splitting requires a minimum applied voltage of 1.23 V (300K), and commercial electrolyzers generally operate at 1.5–1.9 V, which is incom-

patible with state-of-the-art multi-junction solar cells. This requires the solar cells or the electrolyzers to be series connected for their operation voltage to match. Recently, Jia et al. reported a high STH efficiency PV–electrolysis system based on InGaP/GaAs/GaInNAsSb three-junction solar cell. Through connecting two proton exchange membrane (PEM) electrolyzers in series, the electrolyzer unit and photovoltaic unit are tuned to be well matched near the maximum power point of the solar cell. The schematic of the PV–electrolysis system is shown in Figure 10a [100]. Such optimally coupled system fully utilizes the high efficiency three-junction solar cell, and achieves a STH efficiency of over 30%, which is the highest reported to date. However, during 48 h continuous operation, the efficiency drops to near 28%. The author attributed this decrease mostly to the decrease of the PEM electrolyzer performance over time, yet using long-term stable commercial electrolyzers might also lead to reduced efficiency due to their lower Faradaic efficiency. Despite the remarkable solar-to-hydrogen efficiency, the system uses precious materials for the III-V PV cell and electrocatalyst fabrication, making it difficult for commercial setups. The separate configuration of solar cell and electrolyzer component in the PV–electrolysis setup endows the system with better stability and allows the separated component to be optimized for higher performances through series connections and solar concentration. The PV–electrolysis system, in general, shows high STH conversion efficiency and is more mature for industrial operations. However, to achieve large-scale H<sub>2</sub> production, issues of system complexity, high cost, and temperature regulation of PV cells must be considered [96,103].

Photoelectrochemical (PEC) cell is another system configuration for water photoelectrolysis, which combines the solar energy harvesting and water splitting process through immersed semiconductor-based photoelectrodes [104–107]. The PEC system shows great potential in low-cost, large-scale hydrogen production due to its high integration, yet at present is still limited to academic research and lab tests. This is because the photoelectrode materials should satisfy a number of requirements, including wide absorption spectral range, appropriate band alignment, and stability in electrolyte solution [98]. To compensate for the deficiency in materials, photoelectrodes can be coupled to PV cells that provide sufficient voltage bias complementing the voltage shortage of photoelectrodes, forming PV/PEC tandem structures [108,109]. Recently, Young et al. reported a PV/PEC tandem cell with improved semiconductor architectures and reformed growth techniques, achieving STH efficiency over 16% [110]. Through solar-to-hydrogen efficiency modelling of PEC tandem devices, the author decided on the bandgap combination of 1.8/1.2 eV GaInP/GaInAs absorber with a theoretical efficiency of 24%. Such bandgap combinations are achieved via a novel metamorphic growth technique using a compositionally graded buffer (CGB) layer between the junctions. The inverted growth technique and the CGB layer allow the bandgaps of the two junctions to be independently variable, thus maximizing light harvesting by spreading the solar spectrum into the top and bottom sub-cells. However, despite the remarkable efficiency, the system uses expensive III-V semiconductor materials and yields poor long-term stability, with stable operation of only 20 min. Recent research interests are also focused on low-cost and stable transition metal oxides such as TiO<sub>2</sub> and Fe<sub>2</sub>O<sub>3</sub>. Vilanova et al. reported a tandem PV/PEC cell with 50 cm<sup>2</sup> of photoactive area using hematite ( $\alpha$ -Fe<sub>2</sub>O<sub>3</sub>) photoelectrode [111]. The author improved the PEC cell structure, which features an open path for enhanced light harvesting and optimized fluid flow for efficient electrolyte cycle, gas collection, and temperature maintenance under concentrated sunlight. Owing to the compact and optimized design, the tandem PV/PEC cell presented stable operation over 42 days. In a succeeding work, the author expanded the photoactive area to 200 cm<sup>2</sup> through integrating four hematite PEC cells, demonstrating potentials in large-scale hydrogen production, as shown in Figure 10b [112]. Cuprous oxide (Cu<sub>2</sub>O) is also reported as photocathode material in a dual absorber PV/PEC tandem cell with perovskite PV. As is illustrated in Figure 10c, the dual absorbers of PV cell and photocathode are placed back-to-back so that the solar spectrum can be separately and broadly utilized. Particularly, the Au substrate of photocathode is discontinuously deposited for transparency of the Cu<sub>2</sub>O absorber. The system demonstrates unbiased

solar water splitting capability with STH efficiency of 2.5% and potential of performance enhancement based on this configuration [113]. Photoelectrochemical water splitting is still under development, and improvements in photoelectrode materials have become the major challenges for its further development. Present research interests of photoelectrode materials generally focus on the following aspects: (i) elevating visible light harvesting through doping or self-defects, (ii) improving charge transport through structure and morphology engineering, (iii) enhancing operation stability for long-term catalytic applications by applying protective coatings, and (iv) reducing cost by using earth-abundant materials such as transition metal oxides instead of expensive III-V materials.

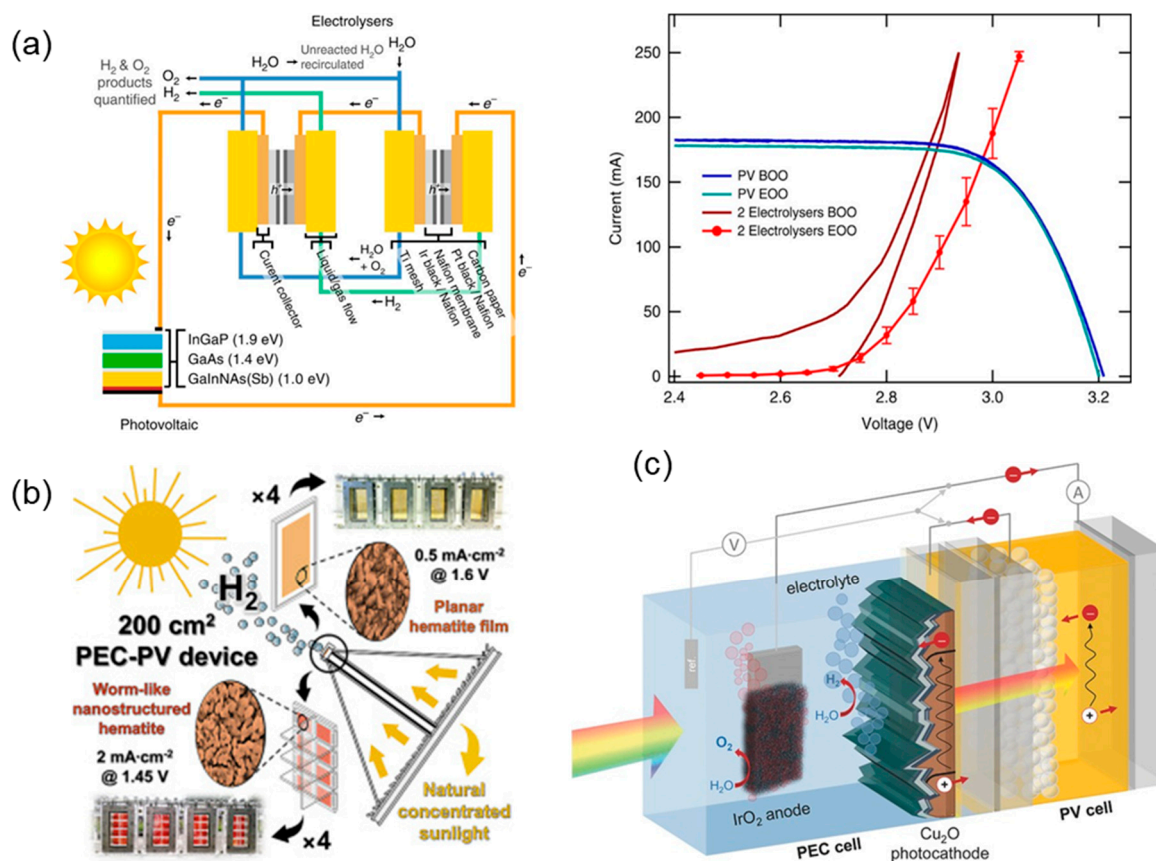


**Figure 10.** (a) Schematics of the PV–electrolysis system and performances of PV cell and proton exchange membrane (PEM) electrolyzer at the beginning and end of operation. (b) Illustration of CoolPEC module for solar water splitting. (c) Schematic of the stacked tandem cell for unbiased water splitting. (a) Reproduced from [100], Copyright 2016, Springer Nature. (b) Reproduced from [112], Copyright 2020, Elsevier. (c) Reproduced from [113], Copyright 2015, Wiley-VCH Verlag GmbH & Co. KGaA, Weinheim.

#### 4. Perspectives

As we have discussed in the main body of this text, energy harvesting technology leads to further improvements in the efficiency and performance of water splitting systems. Because energy harvesting devices, such as piezoelectric, piezo-photoelectric, and pyroelectric devices, are mainly based on ferroelectric properties, the synthesis and employment of materials with appropriate properties are of great importance. Recently, there have been two groups of fascinating materials introduced in the materials research community: (i) metal halide perovskites and (ii) two-dimensional nanomaterials [54,55,82,83,114–116]. Both materials show ferroelectricity, which means that they possess both piezoelectricity and pyroelectricity as well [117–121]. Furthermore, both materials exhibit high light sensitivity and light absorption. These two properties of both materials, ferroelectricity and light

absorption, make them promising candidates for future energy harvesting-assisted water splitting applications. For example, metal halide perovskites can be employed in the water splitting system to induce a piezo-phototronic effect. As the perovskites exhibit extremely a long carrier lifetime and diffusion length, exciton dissociation by the additional electric field by the piezoelectricity will enhance the charge carrier transport to electrodes, leading to improved hydrogen evolution rate [122,123]. Furthermore, to achieve higher efficiency in the water splitting system, utilization of a narrower bandgap is desirable because approximately 50 and 40% of solar spectrum lies in visible and infrared ranges, respectively, which, together with other materials characteristics, makes metal halide perovskites one of the promising materials for energy harvesting-assisted water splitting applications. In terms of 2D nanomaterials, their high surface to volume ratio together with their ferroelectricity make them excellent candidates for water splitting applications [122,123]. Enabled by its high surface to volume ratio together with piezoelectricity or pyroelectricity, a larger amount of H<sub>2</sub> gases can be generated at active sites. In addition, by utilizing Van der Waals force, 2D nanomaterials can be transformed into multi-dimensional materials, such as 0D decorated 2D materials or 3D through stacking of 2D materials, which provides additional functionalities to the devices, such as, photo/electrocatalytic reaction sites by integrating other catalytic materials [55].

Different from triboelectric and pyroelectric (EPP) energy harvesting technologies, which are based on electrolysis of water, the core mechanism of the piezoelectric and pyroelectric (IPP) energy harvesting-assisted water splitting mainly lies in modulating the polarization-induced piezo-/pyro-electric potential to provide favorable energy band bending, which leads to efficient charge carrier transport. Energy band bending mechanism is controllable by adjusting the intensity of input mechanical vibrations or temperature fluctuations, suggesting that we can actively control the amount of H<sub>2</sub> evolution depending on our needs. This controllability makes the energy harvesting technology a powerful method to play a role to improve the water splitting systems. In spite of great potentials of energy harvesting technology to boost water splitting performances, there are underlying mechanisms that need thorough investigations: (i) Comprehensive studies on governing factors of piezoelectric, piezo-phototronic, and pyroelectric effects on water splitting are worth investigating, for example, polarization field versus thickness to determine the optimum space charge region, and interface engineering to reduce charge trapping at the heterojunction. (ii) Together with new materials, design of new device architecture is one of the important factors to be determined. Evolution of 3D printing enables us to design various device structures with enhanced contact areas and efficient charge transport paths in multi-dimensional structures beyond 1D and 2D. (iii) It is timely to conduct experiments on the practical models for mechanical vibration input for piezoelectric and piezo-phototronic energy harvesting-assisted water splitting applications because mechanical vibrations from the environment might have less power than that of the conditions used in simulated situations in the lab environment. (iv) Lastly, we need to further expand these fascinating phenomena to other applications, such as CO<sub>2</sub> reduction and H<sub>2</sub>O<sub>2</sub> production, which will open up new opportunities in the environmental and energy fields.

## 5. Summary

This review has discussed the recent progresses in detail on water splitting systems coupled with energy-harvesting technologies utilizing piezoelectric, piezo-phototronic, pyroelectric, triboelectric, and photovoltaic effects. We summarized water splitting systems with different physical effects in each sub-chapter with detailed examples. These systems can be categorized into two main processes: (i) assisting photo(electro)catalytic reactions through the piezoelectric, piezo-phototronic, and pyroelectric effects by inducing additional potentials for charge separation and transport, or (ii) providing currents and potentials to activate (photo) electrolysis of water through pyroelectric, triboelectric, and photovoltaic effects. Both processes enabled by energy-harvesting technologies demonstrated their promising futures for the future water splitting applications with significantly improved

H<sub>2</sub> and O<sub>2</sub> evolution rates. Finally, in perspectives, we introduced new opportunities from new materials as well as device structure and design. The confronting imminent energy and environment issues need to be mitigated and resolved as soon as possible for the future generations. As a clean and renewable energy source, hydrogen for a major source of energy will realize sustainable society and open up new futures for human beings. Therefore, developing highly efficient renewable energy systems coupled with energy harvesting technology is crucial for sustainable hydrogen production.

**Author Contributions:** J.T., T.L., and S.M. performed literature reviews and wrote the paper under the supervision of Y.C. All authors have read and agreed to the published version of the manuscript.

**Funding:** This work was financially supported by the National Natural Science Foundation of China, grant number 52050410331.

**Institutional Review Board Statement:** Not applicable.

**Informed Consent Statement:** Not applicable.

**Data Availability Statement:** No new data were created or analyzed in this study. Data sharing is not applicable to this article.

**Acknowledgments:** Y.C. would like to thank University of Michigan–Shanghai Jiao Tong University Joint Institution for a support of this work.

**Conflicts of Interest:** The authors declare no conflict of interest.

## References

1. Chu, S.; Majumdar, A. Opportunities and Challenges for a Sustainable Energy Future. *Nature* **2012**, *488*, 294–303. [[CrossRef](#)] [[PubMed](#)]
2. Cox, P.M.; Betts, R.A.; Jones, C.D.; Spall, S.A.; Totterdell, I.J. Acceleration of Global Warming Due to Carbon-Cycle Feedbacks in a Coupled Climate Model. *Nature* **2000**, *408*, 184–187. [[CrossRef](#)]
3. Lee, R. The Outlook for Population Growth. *Science* **2011**, *333*, 569–573. [[CrossRef](#)]
4. Turner, J.A. Sustainable Hydrogen Production. *Science* **2004**, *305*, 972–974. [[CrossRef](#)]
5. Turner, J.A. A Realizable Renewable Energy Future. *Science* **1999**, *285*, 687–689. [[CrossRef](#)]
6. Hosseini, S.E.; Wahid, M.A. Hydrogen Production from Renewable and Sustainable Energy Resources: Promising Green Energy Carrier for Clean Development. *Renew. Sust. Energy Rev.* **2016**, *57*, 850–866. [[CrossRef](#)]
7. Lucia, U. Overview on Fuel Cells. *Renew. Sust. Energy Rev.* **2014**, *30*, 164–169. [[CrossRef](#)]
8. Tee, S.Y.; Win, K.Y.; Teo, W.S.; Koh, L.D.; Liu, S.H.; Teng, C.P.; Han, M.Y. Recent Progress in Energy-Driven Water Splitting. *Adv. Sci.* **2017**, *4*, 1600337. [[CrossRef](#)]
9. Xie, M.Y.; Dunn, S.; Le Boulbar, E.; Bowen, C.R. Pyroelectric Energy Harvesting for Water Splitting. *Int. J. Hydrogen Energy* **2017**, *42*, 23437–23445. [[CrossRef](#)]
10. You, H.L.; Wu, Z.; Zhang, L.H.; Ying, Y.R.; Liu, Y.; Fei, L.F.; Chen, X.X.; Jia, Y.M.; Wang, Y.J.; Wang, F.F.; et al. Harvesting the Vibration Energy of BiFeO<sub>3</sub> Nanosheets for Hydrogen Evolution. *Angew. Chem. Int. Ed.* **2019**, *58*, 11779–11784. [[CrossRef](#)] [[PubMed](#)]
11. Thi, T.P.P.; Yan, Z.; Nick, G.; Hamideh, K.; Phuc, H.D.N.; Zhou, X.F.; Dou, Z.; Zhou, K.C.; Steve, D.; Chris, B. Demonstration of Enhanced Piezo-Catalysis for Hydrogen Generation and Water Treatment at the Ferroelectric Curie Temperature. *Iscience* **2020**, *23*, 101095.
12. Chen, F.; Huang, H.W.; Guo, L.; Zhang, Y.H.; Ma, T.Y. The Role of Polarization in Photocatalysis. *Angew. Chem. Int. Ed.* **2019**, *58*, 10061–10073. [[CrossRef](#)] [[PubMed](#)]
13. Wang, M.Y.; Wang, B.; Huang, F.; Lin, Z.Q. Enabling PIEZOpotential in PIEZOelectric Semiconductors for Enhanced Catalytic Activities. *Angew. Chem. Int. Ed.* **2019**, *58*, 7526–7536. [[CrossRef](#)] [[PubMed](#)]
14. Zhong, Y.; Xia, X.H.; Mai, W.J.; Tu, J.P.; Fan, H.J. Integration of Energy Harvesting and Electrochemical Storage Devices. *Adv. Mater. Technol.* **2017**, *2*, 1700182. [[CrossRef](#)]
15. Zhang, Y.; Xie, M.Y.; Adamaki, V.; Khanbareh, H.; Bowen, C.R. Control of Electro-Chemical Processes Using Energy Harvesting Materials and Devices. *Chem. Soc. Rev.* **2017**, *46*, 7757–7786. [[CrossRef](#)] [[PubMed](#)]
16. Wang, C.; Tian, N.; Ma, T.; Zhang, Y.; Huang, H. Pyroelectric Catalysis. *Nano Energy* **2020**, 105371. [[CrossRef](#)]
17. Kuang, Y.; Kenney, M.J.; Meng, Y.T.; Hung, W.H.; Liu, Y.J.; Huang, J.E.; Prasanna, R.; Li, P.S.; Li, Y.P.; Wang, L.; et al. Solar-Driven, Highly Sustained Splitting of Seawater into Hydrogen and Oxygen Fuels. *Proc. Natl. Acad. Sci. USA* **2019**, *116*, 6624–6629. [[CrossRef](#)]
18. Shin, K.; Park, J.H. Highly Transparent Dual-Sensitized Titanium Dioxide Nanotube Arrays for Spontaneous Solar Water Splitting Tandem Configuration. *ACS Appl. Mater. Interfaces* **2015**, *7*, 18429–18434. [[CrossRef](#)]

19. Niu, S.M.; Wang, X.F.; Yi, F.; Zhou, Y.S.; Wang, Z.L. A Universal Self-Charging System Driven by Random Biomechanical Energy for Sustainable Operation of Mobile Electronics. *Nat. Commun.* **2015**, *6*, 8975. [[CrossRef](#)]
20. Fajrina, N.; Tahir, M. A Critical Review in Strategies to Improve Photocatalytic Water Splitting Towards Hydrogen Production. *Int. J. Hydrogen Energy* **2019**, *44*, 540–577. [[CrossRef](#)]
21. Maeda, K.; Domen, K. Photocatalytic Water Splitting: Recent Progress and Future Challenges. *J. Phys. Chem. Lett.* **2010**, *1*, 2655–2661. [[CrossRef](#)]
22. Hou, B.; Kim, B.-S.; Lee, H.K.H.; Cho, Y.; Giraud, P.; Liu, M.; Zhang, J.; Davies, M.L.; Durrant, J.R.; Tsoi, W.C.; et al. Multi-photon Absorption Stimulated Metal Chalcogenide Quantum Dot Solar Cells under Ambient and Concentrated Irradiance. *Adv. Funct. Mater.* **2020**, *30*, 2004563.
23. Ni, M.; Leung, M.K.H.; Leung, D.Y.C.; Sumathy, K. A Review and Recent Developments in Photocatalytic Water-Splitting Using TiO<sub>2</sub> for Hydrogen Production. *Renew. Sust. Energy Rev.* **2007**, *11*, 401–425. [[CrossRef](#)]
24. Suen, N.T.; Hung, S.F.; Quan, Q.; Zhang, N.; Xu, Y.J.; Chen, H.M. Electrocatalysis for the Oxygen Evolution Reaction: Recent Development and Future Perspectives. *Chem. Soc. Rev.* **2017**, *46*, 337–365. [[CrossRef](#)] [[PubMed](#)]
25. Greeley, J.; Jaramillo, T.F.; Bonde, J.; Chorkendorff, I.B.; Norskov, J.K. Computational High-Throughput Screening of Electrocatalytic Materials for Hydrogen Evolution. *Nat. Mater.* **2006**, *5*, 909–913. [[CrossRef](#)] [[PubMed](#)]
26. Zhu, J.; Hu, L.S.; Zhao, P.X.; Lee, L.Y.S.; Wong, K.Y. Recent Advances in Electrocatalytic Hydrogen Evolution Using Nanoparticles. *Chem. Rev.* **2020**, *120*, 851–918. [[CrossRef](#)]
27. Caserta, G.; Cervigni, T. Piezoelectric Theory of Enzymic Catalysis as Inferred from the Electromechanochemical Principles of Bioenergetics. *Proc. Natl. Acad. Sci. USA* **1974**, *71*, 4421–4424. [[CrossRef](#)]
28. Shi, J.; Starr, M.B.; Xiang, H.; Hara, Y.; Anderson, M.A.; Seo, J.H.; Ma, Z.Q.; Wang, X.D. Interface Engineering by Piezoelectric Potential in ZnO-Based Photoelectrochemical Anode. *Nano Lett.* **2011**, *11*, 5587–5593. [[CrossRef](#)]
29. Li, H.D.; Sang, Y.H.; Chang, S.J.; Huang, X.; Zhang, Y.; Yang, R.S.; Jiang, H.D.; Liu, H.; Wang, Z.L. Enhanced Ferroelectric-Nanocrystal-Based Hybrid Photocatalysis by Ultrasonic-Wave-Generated Piezophototronic Effect. *Nano Lett.* **2015**, *15*, 2372–2379. [[CrossRef](#)]
30. Giocondi, J.L.; Rohrer, G.S. Spatial Separation of Photochemical Oxidation and Reduction Reactions on the Surface of Ferroelectric BaTiO<sub>3</sub>. *J. Phys. Chem. B* **2001**, *105*, 8275–8277. [[CrossRef](#)]
31. Kakekhani, A.; Ismail-Beigi, S. Ferroelectric Oxide Surface Chemistry: Water Splitting via Pyroelectricity. *J. Mater. Chem. A* **2016**, *4*, 5235–5246. [[CrossRef](#)]
32. Starr, M.B.; Wang, X.D. Coupling of Piezoelectric Effect with Electrochemical Processes. *Nano Energy* **2015**, *14*, 296–311. [[CrossRef](#)]
33. Hong, K.S.; Xu, H.F.; Konishi, H.; Li, X.C. Direct Water Splitting Through Vibrating Piezoelectric Microfibers in Water. *J. Phys. Chem. Lett.* **2010**, *1*, 997–1002. [[CrossRef](#)]
34. Starr, M.B.; Shi, J.; Wang, X.D. Piezopotential-Driven Redox Reactions at the Surface of Piezoelectric Materials. *Angew. Chem. Int. Ed.* **2012**, *51*, 5962–5966. [[CrossRef](#)] [[PubMed](#)]
35. Hong, K.S.; Xu, H.F.; Konishi, H.; Li, X.C. Piezoelectrochemical Effect: A New Mechanism for Azo Dye Decolorization in Aqueous Solution through Vibrating Piezoelectric Microfibers. *J. Phys. Chem. C* **2012**, *116*, 13045–13051. [[CrossRef](#)]
36. Tan, C.F.; Ong, W.L.; Ho, G.W. Self-Biased Hybrid Piezoelectric-Photoelectrochemical Cell with Photocatalytic Functionalities. *ACS Nano* **2015**, *9*, 7661–7670. [[CrossRef](#)]
37. Xue, X.Y.; Zang, W.L.; Deng, P.; Wang, Q.; Xing, L.L.; Zhang, Y.; Wang, Z.L. Piezo-Potential Enhanced Photocatalytic Degradation of Organic Dye Using ZnO Nanowires. *Nano Energy* **2015**, *13*, 414–422. [[CrossRef](#)]
38. Wu, J.M.; Chang, W.E.; Chang, Y.T.; Chang, C.K. Piezo-Catalytic Effect on the Enhancement of the Ultra-High Degradation Activity in the Dark by Single- and Few-Layers MoS<sub>2</sub> Nanoflowers. *Adv. Mater.* **2016**, *28*, 3718–3725. [[CrossRef](#)]
39. Huang, H.W.; Tu, S.C.; Zeng, C.; Zhang, T.R.; Reshak, A.H.; Zhang, Y.H. Macroscopic Polarization Enhancement Promoting Photo- and Piezoelectric-Induced Charge Separation and Molecular Oxygen Activation. *Angew. Chem. Int. Ed.* **2017**, *56*, 11860–11864. [[CrossRef](#)]
40. Feng, Y.W.; Ling, L.L.; Wang, Y.X.; Xu, Z.M.; Cao, F.L.; Li, H.X.; Bian, Z.F. Engineering Spherical Lead Zirconate Titanate to Explore the Essence of Piezo-Catalysis. *Nano Energy* **2017**, *40*, 481–486. [[CrossRef](#)]
41. Handzlik, G.; Koziel, M.; Olejniczak, A.; Sieklucka, B.; Pinkowicz, D. Cyanide vs. Zr<sup>2+</sup> “Magnetic Arm Wrestling”: Mn-II-Nb-IV and Mn-II-Mo-IV Magnetic Coordination Polymers with Mixed Bridging. *Chem. Commun.* **2017**, *53*, 9753–9756. [[CrossRef](#)]
42. Voiry, D.; Fullon, R.; Yang, J.E.; Silva, C.D.C.E.; Kappera, R.; Bozkurt, I.; Kaplan, D.; Lagos, M.J.; Batson, P.E.; Gupta, G.; et al. The Role of Electronic Coupling Between Substrate and 2D MoS<sub>2</sub> Nanosheets in Electrocatalytic Production of Hydrogen. *Nat. Mater.* **2016**, *15*, 1003–1009. [[CrossRef](#)]
43. Hinnemann, B.; Moses, P.G.; Bonde, J.; Jorgensen, K.P.; Nielsen, J.H.; Horch, S.; Chorkendorff, I.; Norskov, J.K. Biomimetic Hydrogen Evolution: MoS<sub>2</sub> Nanoparticles as Catalyst for Hydrogen Evolution. *J. Am. Chem. Soc.* **2005**, *127*, 5308–5309. [[CrossRef](#)] [[PubMed](#)]
44. Li, H.; Tan, Y.; Liu, P.; Guo, C.; Luo, M.; Han, J.; Lin, T.; Huang, F.; Chen, M. Atomic-Sized Pores Enhanced Electrocatalysis of TaS<sub>2</sub> Nanosheets for Hydrogen Evolution. *Adv. Mater.* **2016**, *28*, 8945–8949. [[CrossRef](#)]
45. Sang, Y.H.; Zhao, Z.H.; Zhao, M.W.; Hao, P.; Leng, Y.H.; Liu, H. From UV to Near-Infrared, WS<sub>2</sub> Nanosheet: A Novel Photocatalyst for Full Solar Light Spectrum Photodegradation. *Adv. Mater.* **2015**, *27*, 363–369. [[CrossRef](#)] [[PubMed](#)]

46. Lu, Q.P.; Yu, Y.F.; Ma, Q.L.; Chen, B.; Zhang, H. 2D Transition-Metal-Dichalcogenide-Nanosheet-Based Composites for Photocatalytic and Electrocatalytic Hydrogen Evolution Reactions. *Adv. Mater.* **2016**, *28*, 1917–1933. [[CrossRef](#)] [[PubMed](#)]
47. Wu, W.; Wang, L.; Li, Y.; Zhang, F.; Lin, L.; Niu, S.; Chenet, D.; Zhang, X.; Hao, Y.; Heinz, T.F.; et al. Piezoelectricity of Single-Atomic-Layer MoS<sub>2</sub> for Energy Conversion and Piezotronics. *Nature* **2014**, *514*, 470–474. [[CrossRef](#)] [[PubMed](#)]
48. Zhu, H.Y.; Wang, Y.; Xiao, J.; Liu, M.; Xiong, S.M.; Wong, Z.J.; Ye, Z.L.; Ye, Y.; Yin, X.B.; Zhang, X. Observation of Piezoelectricity in Free-Standing Monolayer MoS<sub>2</sub>. *Nat. Nanotechnol.* **2015**, *10*, 151–155. [[CrossRef](#)]
49. Jeong, H.; Oh, H.M.; Gokarna, A.; Kim, H.; Yun, S.J.; Han, G.H.; Jeong, M.S.; Lee, Y.H.; Lerondel, G. Integrated Freestanding Two-dimensional Transition Metal Dichalcogenides. *Adv. Mater.* **2017**, *29*, 1700308. [[CrossRef](#)]
50. Liu, Y.D.; Guo, J.M.; Yu, A.F.; Zhang, Y.; Kou, J.Z.; Zhang, K.; Wen, R.M.; Zhang, Y.; Zhai, J.Y.; Wang, Z.L. Magnetic-Induced-Piezopotential Gated MoS<sub>2</sub> Field-Effect Transistor at Room Temperature. *Adv. Mater.* **2018**, *30*, 1704524. [[CrossRef](#)]
51. Lee, J.H.; Park, J.Y.; Cho, E.B.; Kim, T.Y.; Han, S.A.; Kim, T.H.; Liu, Y.; Kim, S.K.; Roh, C.J.; Yoon, H.J.; et al. Reliable Piezoelectricity in Bilayer WSe<sub>2</sub> for Piezoelectric Nanogenerators. *Adv. Mater.* **2017**, *29*, 1606667. [[CrossRef](#)] [[PubMed](#)]
52. Esfahani, E.N.; Li, T.; Huang, B.; Xu, X.D.; Li, J.Y. Piezoelectricity of Atomically Thin WSe<sub>2</sub> via Laterally Excited Scanning Probe Microscopy. *Nano Energy* **2018**, *52*, 117–122. [[CrossRef](#)]
53. Bollinger, M.V.; Lauritsen, J.V.; Jacobsen, K.W.; Norskov, J.K.; Helveg, S.; Besenbacher, F. One-Dimensional Metallic Edge States in MoS<sub>2</sub>. *Phys. Rev. Lett.* **2001**, *87*, 196803. [[CrossRef](#)] [[PubMed](#)]
54. Li, S.; Zhao, Z.C.; Yu, D.F.; Zhao, J.Z.; Su, Y.P.; Liu, Y.; Lin, Y.H.; Liu, W.S.; Xu, H.; Zhang, Z.T. Few-Layer Transition Metal Dichalcogenides (MoS<sub>2</sub>, WS<sub>2</sub>, and WSe<sub>2</sub>) for Water Splitting and Degradation of Organic Pollutants: Understanding the Piezocatalytic Effect. *Nano Energy* **2019**, *66*, 104083. [[CrossRef](#)]
55. Feng, W.H.; Yuan, J.; Gao, F.; Weng, B.; Hu, W.T.; Lei, Y.H.; Huang, X.Y.; Yang, L.; Shen, J.; Xu, D.; et al. Piezopotential-Driven Simulated Electrocatalytic Nanosystem of Ultrasmall MoC Quantum Dots Encapsulated in Ultrathin N-Doped Graphene Vesicles for Superhigh H<sub>2</sub> Production from Pure Water. *Nano Energy* **2020**, *75*, 104990. [[CrossRef](#)]
56. Zhao, Y.; Fang, Z.B.; Feng, W.H.; Wang, K.Q.; Huang, X.Y.; Liu, P. Hydrogen Production from Pure Water via Piezoelectric-assisted Visible-light Photocatalysis of CdS Nanorod Arrays. *ChemCatChem* **2018**, *10*, 3397–3401. [[CrossRef](#)]
57. Sasikala, R.; Jayakumar, O.D.; Kulshreshtha, S.K. Enhanced Hydrogen Generation by Particles during Sonochemical Decomposition of Water. *Ultrason. Sonochem.* **2007**, *14*, 153–156. [[CrossRef](#)]
58. Zhang, J.; Wu, Z.; Jia, Y.M.; Kan, J.W.; Cheng, G.M. Piezoelectric Bimorph Cantilever for Vibration-Producing-Hydrogen. *Sensors* **2013**, *13*, 367–374. [[CrossRef](#)]
59. Pan, L.; Sun, S.C.; Chen, Y.; Wang, P.H.; Wang, J.Y.; Zhang, X.W.; Zou, J.J.; Wang, Z.L. Advances in Piezo-Phototronic Effect Enhanced Photocatalysis and Photoelectrocatalysis. *Adv. Energy Mater.* **2020**, *10*, 2000214. [[CrossRef](#)]
60. Zhang, Y.; Liu, Y.; Wang, Z.L. Fundamental Theory of Piezotronics. *Adv. Mater.* **2011**, *23*, 3004. [[CrossRef](#)]
61. Wang, Z.L. Progress in Piezotronics and Piezo-Phototronics. *Adv. Mater.* **2012**, *24*, 4632. [[CrossRef](#)] [[PubMed](#)]
62. Yu, R.; Dong, L.; Pan, C.; Niu, S.; Liu, H.; Liu, W.; Chua, S.; Chi, D.; Wang, Z.L. Piezotronic Effect on the Transport Properties of GaN Nanobelts for Active Flexible Electronics. *Adv. Mater.* **2012**, *24*, 3532. [[CrossRef](#)] [[PubMed](#)]
63. Wang, Y.C.; Wu, J.M. Effect of Controlled Oxygen Vacancy on H<sub>2</sub>-Production through the Piezocatalysis and Piezophototronics of Ferroelectric R3C ZnSnO<sub>3</sub> Nanowires. *Adv. Funct. Mater.* **2020**, *30*, 1907619. [[CrossRef](#)]
64. Cho, Y.; Giraud, P.; Hou, B.; Lee, Y.W.; Hong, J.; Lee, S.; Pak, S.; Lee, J.; Jang, J.E.; Morris, S.M.; et al. Charge Transport Modulation of a Flexible Quantum Dot Solar Cell Using a Piezoelectric Effect. *Adv. Energy Mater.* **2018**, *8*, 1700809. [[CrossRef](#)]
65. Chen, Y.; Wang, L.; Gao, R.J.; Zhang, Y.C.; Pan, L.; Huang, C.Y.; Liu, K.; Chang, X.Y.; Zhang, X.W.; Zou, J.J. Polarization-Enhanced direct Z-scheme ZnO-WO<sub>3-x</sub> Nanorod Arrays for Efficient Piezoelectric-Photoelectrochemical Water Splitting. *Appl. Catal. B-Environ.* **2019**, *259*, 118079. [[CrossRef](#)]
66. Ma, J.P.; Ren, J.; Jia, Y.M.; Wu, Z.; Chen, L.; Haugen, N.O.; Huang, H.T.; Liu, Y.S. High Efficiency Bi-Harvesting Light/Vibration Energy Using Piezoelectric Zinc Oxide Nanorods for Dye Decomposition. *Nano Energy* **2019**, *62*, 376–383. [[CrossRef](#)]
67. Hong, D.Y.; Zang, W.L.; Guo, X.; Fu, Y.M.; He, H.X.; Sun, J.; Xing, L.L.; Liu, B.D.; Xue, X.Y. High Piezo-photocatalytic Efficiency of CuS/ZnO Nanowires Using Both Solar and Mechanical Energy for Degrading Organic Dye. *ACS Appl. Mater. Interfaces* **2016**, *8*, 21302–21314. [[CrossRef](#)]
68. Singh, S.; Khare, N. Coupling of Piezoelectric, Semiconducting and Photoexcitation Properties in NaNbO<sub>3</sub> Nanostructures for Controlling Electrical Transport: Realizing an Efficient Piezo-Photoanode and Piezo-Photocatalyst. *Nano Energy* **2017**, *38*, 335–341. [[CrossRef](#)]
69. Yu, D.F.; Liu, Z.H.; Zhang, J.M.; Li, S.; Zhao, Z.C.; Zhu, L.F.; Liu, W.S.; Lin, Y.H.; Liu, H.; Zhang, Z.T. Enhanced Catalytic Performance by Multi-Field Coupling in KNbO<sub>3</sub> Nanostructures: Piezo-Photocatalytic and Ferro-Photoelectrochemical Effects. *Nano Energy* **2019**, *58*, 695–705. [[CrossRef](#)]
70. Yang, Y.; Guo, W.X.; Pradel, K.C.; Zhu, G.; Zhou, Y.S.; Zhang, Y.; Hu, Y.F.; Lin, L.; Wang, Z.L. Pyroelectric Nanogenerators for Harvesting Thermoelectric Energy. *Nano Lett.* **2012**, *12*, 2833–2838. [[CrossRef](#)]
71. Pandya, S.; Velarde, G.; Zhang, L.; Wilbur, J.D.; Smith, A.; Hanrahan, B.; Dames, C.; Martin, L.W. New Approach to Waste-Heat Energy Harvesting: Pyroelectric Energy Conversion. *NPG Asia Mater.* **2019**, *11*, 26. [[CrossRef](#)]
72. Bowen, C.R.; Taylor, J.; LeBoulbar, E.; Zabek, D.; Chauhan, A.; Vaish, R. Pyroelectric Materials and Devices for Energy Harvesting Applications. *Energy Environ. Sci.* **2014**, *7*, 3836–3856. [[CrossRef](#)]

73. Fang, J.; Frederich, H.; Pilon, L. Harvesting Nanoscale Thermal Radiation Using Pyroelectric Materials. *J. Heat Transf.* **2010**, *132*, 092701. [[CrossRef](#)]
74. Huang, K.; Wang, J.B.; Zhong, X.L.; Liu, B.L.; Chen, T.; Zhou, Y.C. Significant Polarization Variation Near Room Temperature of  $\text{Ba}_{0.65}\text{Sr}_{0.35}\text{TiO}_3$  Thin Films for Pyroelectric Energy Harvesting. *Sens. Actuators B Chem.* **2012**, *169*, 208–212. [[CrossRef](#)]
75. Xu, X.L.; Xiao, L.B.; Jia, Y.M.; Wu, Z.; Wang, F.F.; Wang, Y.J.; Haugen, N.O.; Huang, H.T. Pyro-Catalytic Hydrogen Evolution by  $\text{Ba}_{0.7}\text{Sr}_{0.3}\text{TiO}_3$  Nanoparticles: Harvesting Cold-Hot Alternation Energy Near Room-Temperature. *Energy Environ. Sci.* **2018**, *11*, 2198–2207. [[CrossRef](#)]
76. Belitz, R.; Meisner, P.; Coeler, M.; Wunderwald, U.; Friedrich, J.; Zosel, J.; Schelter, M.; Jachalke, S.; Mehner, E. Waste Heat Energy Harvesting by use of  $\text{BaTiO}_3$  for Pyroelectric Hydrogen Generation. *Energy Harvest. Syst.* **2017**, *4*, 107–113. [[CrossRef](#)]
77. Kakekhani, A.; Ismail-Beigi, S.; Altman, E.I. Ferroelectrics: A Pathway to Switchable Surface Chemistry and Catalysis. *Surf. Sci.* **2016**, *650*, 302–316. [[CrossRef](#)]
78. Zhang, Y.; Kumar, S.; Marken, F.; Krasny, M.; Roake, E.; Eslava, S.; Dunn, S.; Da Como, E.; Bowen, C.R. Pyro-Electrolytic Water Splitting for Hydrogen Generation. *Nano Energy* **2019**, *58*, 183–191. [[CrossRef](#)]
79. Kakekhani, A.; Ismail-Beigi, S. Ferroelectric-Based Catalysis: Switchable Surface Chemistry. *ACS Catal.* **2015**, *5*, 4537–4545. [[CrossRef](#)]
80. Kakekhani, A.; Ismail-Beigi, S. Polarization-Driven Catalysis via Ferroelectric Oxide Surfaces. *Phys. Chem. Chem. Phys.* **2016**, *18*, 19676–19695. [[CrossRef](#)]
81. You, H.L.; Jia, Y.M.; Wu, Z.; Wang, F.F.; Huang, H.T.; Wang, Y. Room-Temperature Pyro-Catalytic Hydrogen Generation of 2D Few-Layer Black Phosphorene under Cold-Hot Alternation. *Nat. Commun.* **2018**, *9*, 2889. [[CrossRef](#)] [[PubMed](#)]
82. Guan, Z.; Hu, H.; Shen, X.W.; Xiang, P.H.; Zhong, N.; Chu, J.H.; Duan, C.G. Recent Progress in Two-Dimensional Ferroelectric Materials. *Adv. Electron. Mater.* **2020**, *6*, 190018. [[CrossRef](#)]
83. Sa, B.S.; Li, Y.L.; Qi, J.S.; Ahuja, R.; Sun, Z.M. Strain Engineering for Phosphorene: The Potential Application as a Photocatalyst. *J. Phys. Chem. C* **2014**, *118*, 26560–26568. [[CrossRef](#)]
84. Jiao, Y.; Zheng, Y.; Jaroniec, M.T.; Qiao, S.Z. Design of Electrocatalysts for Oxygen- and Hydrogen-Involving Energy Conversion Reactions. *Chem. Soc. Rev.* **2015**, *44*, 2060–2086. [[CrossRef](#)]
85. Fan, F.R.; Tian, Z.Q.; Wang, Z.L. Flexible Triboelectric Generator! *Nano Energy* **2012**, *1*, 328–334. [[CrossRef](#)]
86. Cho, Y.; Park, J.B.; Kim, B.S.; Lee, J.; Hong, W.K.; Park, I.K.; Jang, J.E.; Sohn, J.I.; Cha, S.; Kim, J.M. Enhanced Energy Harvesting Based on Surface Morphology Engineering of P(VDF-TrFE) Film. *Nano Energy* **2015**, *16*, 524–532. [[CrossRef](#)]
87. Cho, Y.; Ahn, D.; Park, J.B.; Pak, S.; Lee, S.; Jun, B.O.; Hong, J.; Lee, S.Y.; Jang, J.E.; Hong, J.; et al. Enhanced Ferroelectric Property of P(VDF-TrFE-CTFE) Film Using Room-Temperature Crystallization for High-Performance Ferroelectric Device Applications. *Adv. Electron. Mater.* **2016**, *2*, 1600225. [[CrossRef](#)]
88. Cho, Y.; Pak, S.; Lee, Y.G.; Hwang, J.S.; Giraud, P.; An, G.H.; Cha, S. Hybrid Smart Fiber with Spontaneous Self-Charging Mechanism for Sustainable Wearable Electronics. *Adv. Funct. Mater.* **2020**, *30*, 1908479. [[CrossRef](#)]
89. Cho, Y.; Lee, S.; Hong, J.; Pak, S.; Hou, B.; Lee, Y.W.; Jang, J.E.; Im, H.; Sohn, J.I.; Cha, S.; et al. Sustainable Hybrid Energy Harvester Based on Air Stable Quantum Dot Solar Cells and Triboelectric Nanogenerator. *J. Mater. Chem. A* **2018**, *6*, 12440–12446. [[CrossRef](#)]
90. Wei, A.M.; Xie, X.K.; Wen, Z.; Zheng, H.C.; Lan, H.W.; Shao, H.Y.; Sun, X.H.; Zhong, J.; Lee, S.T. Triboelectric Nanogenerator Driven Self-Powered Photoelectrochemical Water Splitting Based on Hematite Photoanodes. *ACS Nano* **2018**, *12*, 8625–8632. [[CrossRef](#)]
91. Zhou, W.J.; Yin, Z.Y.; Du, Y.P.; Huang, X.; Zeng, Z.Y.; Fan, Z.X.; Liu, H.; Wang, J.Y.; Zhang, H. Synthesis of Few-Layer  $\text{MoS}_2$  Nanosheet-Coated  $\text{TiO}_2$  Nanobelt Heterostructures for Enhanced Photocatalytic Activities. *Small* **2013**, *9*, 140–147. [[CrossRef](#)] [[PubMed](#)]
92. Li, T.; Xu, Y.; Xing, F.; Cao, X.; Bian, J.; Wang, N.; Wang, Z.L. Boosting Photoelectrochemical Water Splitting by TENG-Charged Li-Ion Battery. *Adv. Energy Mater.* **2017**, *7*, 1700124. [[CrossRef](#)]
93. Pu, Y.C.; Wang, G.M.; Chang, K.D.; Ling, Y.C.; Lin, Y.K.; Fitzmorris, B.C.; Liu, C.M.; Lu, X.H.; Tong, Y.X.; Zhang, J.Z.; et al. Au Nanostructure-Decorated  $\text{TiO}_2$  Nanowires Exhibiting Photoactivity Across Entire UV-visible Region for Photoelectrochemical Water Splitting. *Nano Lett.* **2013**, *13*, 3817–3823. [[CrossRef](#)] [[PubMed](#)]
94. Song, P.Y.; Kuang, S.Y.; Panwar, N.; Yang, G.; Tng, D.J.H.; Tjin, S.C.; Ng, W.J.; Majid, M.B.; Zhu, G.; Yong, K.T.; et al. A Self-Powered Implantable Drug-Delivery System Using Biokinetic Energy. *Adv. Mater.* **2017**, *29*, 1605668. [[CrossRef](#)] [[PubMed](#)]
95. Fujishima, A.; Honda, K. Electrochemical Photolysis of Water at a Semiconductor Electrode. *Nature* **1972**, *238*, 37–38. [[CrossRef](#)]
96. Ardo, S.; Rivas, D.F.; Modestino, M.A.; Greiving, V.S.; Abdi, F.F.; Alarcon Llado, E.; Artero, V.; Ayers, K.; Battaglia, C.; Becker, J.P.; et al. Pathways to Electrochemical Solar-Hydrogen Technologies. *Energy Environ. Sci.* **2018**, *11*, 2768–2783. [[CrossRef](#)]
97. Dotan, H. Beating the Efficiency of Photovoltaics-Powered Electrolysis with Tandem Cell Photoelectrolysis. *ACS Energy Lett.* **2017**, *2*, 45–51.
98. Luo, J.S.; Im, J.H.; Mayer, M.T.; Schreier, M.; Nazeeruddin, M.K.; Park, N.G.; Tilley, S.D.; Fan, H.J.; Gratzel, M. Water Photolysis at 12.3% Efficiency via Perovskite Photovoltaics and Earth-Abundant Catalysts. *Science* **2014**, *345*, 1593–1596. [[CrossRef](#)]
99. Bonke, S.A.; Wiechen, M.; MacFarlane, D.R.; Spiccia, L. Renewable Fuels from Concentrated Solar Power: Towards Practical Artificial Photosynthesis. *Energy Environ. Sci.* **2015**, *8*, 2791–2796. [[CrossRef](#)]

100. Jia, J.Y.; Seitz, L.C.; Benck, J.D.; Huo, Y.J.; Chen, Y.S.; Ng, J.W.D.; Bilir, T.; Harris, J.S.; Jaramillo, T.F. Solar Water Splitting by Photovoltaic-Electrolysis with a Solar-to-Hydrogen Efficiency over 30%. *Nat. Commun.* **2016**, *7*, 13237. [[CrossRef](#)]
101. Ota, Y.; Yamashita, D.; Nakao, H.; Yonezawa, Y.; Nakashima, Y.; Ebe, H.; Inagaki, M.; Mikami, R.; Abiko, Y.; Iwasaki, T.; et al. Highly Efficient 470 W Solar-to-Hydrogen Conversion System Based on Concentrator Photovoltaic Modules with Dynamic Control of Operating Point. *Appl. Phys. Express* **2018**, *11*, 077101. [[CrossRef](#)]
102. Nakamura, A.; Ota, Y.; Koike, K.; Hidaka, Y.; Nishioka, K.; Sugiyama, M.; Fujii, K. A 24.4% Solar to Hydrogen Energy Conversion Efficiency by Combining Concentrator Photovoltaic Modules and Electrochemical cells. *Appl. Phys. Express* **2015**, *8*, 107101. [[CrossRef](#)]
103. Tournet, J.; Lee, Y.; Krishna, S.K.; Tan, H.H.; Jagadish, C. III-V Semiconductor Materials for Solar Hydrogen Production: Status and Prospects. *ACS Energy Lett.* **2020**, *5*, 611–622. [[CrossRef](#)]
104. Yamada, Y.; Matsuki, N.; Ohmori, T.; Mametsuka, H.; Kondo, M.; Matsuda, A.; Suzuki, E. One Chip Photovoltaic Water Electrolysis Device. *Int. J. Hydrogen Energy* **2003**, *28*, 1167–1169. [[CrossRef](#)]
105. Hu, S.; Xiang, C.X.; Haussener, S.; Berger, A.D.; Lewis, N.S. An Analysis of the Optimal Band Gaps of Light Absorbers in Integrated Tandem Photoelectrochemical Water-Splitting Systems. *Energy Environ. Sci.* **2013**, *6*, 2984–2993. [[CrossRef](#)]
106. Lichterman, M.F.; Sun, K.; Hu, S.; Zhou, X.H.; McDowell, M.T.; Shaner, M.R.; Richter, M.H.; Crumlin, E.J.; Carim, A.I.; Saadi, F.H.; et al. Protection of Inorganic Semiconductors for Sustained, Efficient Photoelectrochemical Water Oxidation. *Catal. Today* **2016**, *262*, 11–23. [[CrossRef](#)]
107. Bae, D.; Pedersen, T.; Seger, B.; Iandolo, B.; Hansen, O.; Vesborg, P.C.K.; Chorkendorff, I. Carrier-Selective P- and N-Contacts for Efficient and Stable Photocatalytic Water Reduction. *Catal. Today* **2017**, *290*, 59–64. [[CrossRef](#)]
108. Zhang, K.; Ma, M.; Li, P.; Wang, D.H.; Park, J.H. Water Splitting Progress in Tandem Devices: Moving Photolysis beyond Electrolysis. *Adv. Energy Mater.* **2016**, *6*, 1600602. [[CrossRef](#)]
109. Fountaine, K.T.; Lewerenz, H.J.; Atwater, H.A. Efficiency Limits for Photoelectrochemical Water-Splitting. *Nat. Commun.* **2016**, *7*, 13706. [[CrossRef](#)]
110. Young, J.L.; Steiner, M.A.; Doscher, H.; France, R.M.; Turner, J.A.; Deutsch, T.G. Direct Solar-to-Hydrogen Conversion via Inverted Metamorphic Multi-Junction Semiconductor Architectures. *Nat. Energy* **2017**, *2*, 17028. [[CrossRef](#)]
111. Vilanova, A.; Lopes, T.; Spenke, C.; Wullenkord, M.; Mendes, A. Optimized Photoelectrochemical Tandem Cell for Solar Water Splitting. *Energy Storage Mater.* **2018**, *13*, 175–188. [[CrossRef](#)]
112. Vilanova, A.; Dias, P.; Azevedo, J.; Wullenkord, M.; Spenke, C.; Lopes, T.; Mendes, A. Solar Water Splitting under Natural Concentrated Sunlight Using a 200 cm<sup>2</sup> Photoelectrochemical-Photovoltaic Device. *J. Power Sources* **2020**, *454*, 227890. [[CrossRef](#)]
113. Dias, P.; Schreier, M.; Tilley, S.D.; Luo, J.S.; Azevedo, J.; Andrade, L.; Bi, D.Q.; Hagfeldt, A.; Mendes, A.; Gratzel, M.; et al. Transparent Cuprous Oxide Photocathode Enabling a Stacked Tandem Cell for Unbiased Water Splitting. *Adv. Energy Mater.* **2015**, *5*, 1501537. [[CrossRef](#)]
114. Chen, J.; Dong, C.; Idriss, H.; Mohammed, O.F.; Bakr, O.M. Metal Halide Perovskites for Solar-to-Chemical Fuel Conversion. *Adv. Energy Mater.* **2020**, *10*, 1902433. [[CrossRef](#)]
115. Zhang, W.; Eperon, G.E.; Snaith, H.J. Metal Halide Perovskites for Energy Applications. *Nat. Energy* **2016**, *1*, 1–8. [[CrossRef](#)]
116. Leite, M.S.; Saliba, M.; Thomas, K.G.; Manoj, B.; Kamat, P.V. Energy Spotlight: Advances in Metal Halide Perovskites, Photoactivated Catalysis, and Organic Photovoltaics. *ACS Energy Lett.* **2020**, *5*, 3876–3878. [[CrossRef](#)]
117. Howard, J.M.; Lahoti, R.; Leite, M.S. Imaging Metal Halide Perovskites Material and Properties at the Nanoscale. *Adv. Energy Mater.* **2019**, *10*, 1903161. [[CrossRef](#)]
118. Jella, V.; Ippili, S.; Eom, J.H.; Pammi, S.V.N.; Jung, J.S.; Tran, V.D.; Nguyen, V.H.; Kirakosyan, A.; Yun, S.; Kim, D.; et al. A Comprehensive Review of Flexible Piezoelectric Generators Based on Organic-Inorganic Metal Halide Perovskites. *Nano Energy* **2019**, *57*, 74–93. [[CrossRef](#)]
119. Park, H.; Ha, C.; Lee, J.H. Advances in Piezoelectric Halide Perovskites for Energy Harvesting Applications. *J. Mater. Chem. A* **2020**, *8*, 24353–24367. [[CrossRef](#)]
120. Cui, C.; Xue, F.; Hu, W.J.; Li, L.J. Two-Dimensional Materials with Piezoelectric and Ferroelectric Functionalities. *NPJ 2D Mater. Appl.* **2018**, *2*, 1–14. [[CrossRef](#)]
121. Hinchet, R.; Khan, U.; Falconi, C.; Kim, S.W. Piezoelectric Properties in Two-Dimensional Materials: Simulations and Experiments. *Mater. Today* **2018**, *21*, 611–630. [[CrossRef](#)]
122. De Quilettes, D.W.; Vorpahl, S.M.; Stranks, S.D.; Nagaoka, H.; Eperon, G.E.; Ziffer, M.E.; Snaith, H.J.; Ginger, D.S. Impact of Microstructure on Local Carrier Lifetime in Perovskite Solar Cells. *Science* **2015**, *348*, 683–686. [[CrossRef](#)] [[PubMed](#)]
123. Stranks, S.D.; Eperon, G.E.; Grancini, G.; Menelaou, C.; Alcocer, M.J.; Leijtens, T.; Herz, L.M.; Petrozza, A.; Snaith, H.J. Electron-Hole Diffusion Lengths Exceeding 1 Micrometer in an Organometal Trihalide Perovskite Absorber. *Science* **2013**, *342*, 341–344. [[CrossRef](#)] [[PubMed](#)]